Ministry of Higher Education and Scientific Research
University of Babylon
College of Science
Department of Physics

High Reflectance Nanolayers Prepared from (Al-Ni-Cr) Alloy for Laser Resonator via Thermal Evaporation Technique

A Thesis

Submitted to the Council of Physics Department, College of Science, University of Babylon in Partial Fulfilment of the Requirements for theDegree of Master of Science in Physics

By

Huda Raad Abdulridha Mohammed

B.Sc. in Physics /2017

Supervised by

Prof. Dr.
Abdulazeez O. Mousa Al-Ogaili

Prof.Dr.
Khalid Haneen Abass Hassan

2021A.D. **1443A.H.**

بسم الله الرحمن الرحيم

﴿ يَـٰٓأَيُّهَا ٱلَّذِينَ ءَامَنُوٓاْ إِذَا قِيلَ لَكُمۡ تَفَسَّحُواْ فِي ٱلۡمَجَٰلِسِ فَٱفۡسَحُواْ يَفۡسَحِ ٱللَّهُ لَكُمۡۖ وَإِذَا قِيلَ ٱنشُزُواْ فَٱنشُزُواْ يَرۡفَعِ ٱللَّهُ ٱلَّذِينَ ءَامَنُواْ مِنكُمۡ وَٱلَّذِينَ أُوتُواْ ٱلۡعِلۡمَ دَرَجَٰتٖۚ وَٱللَّهُ بِمَا تَعۡمَلُونَ خَبِيرٞ ﴾

صَدَقَ اللهُ العَظِيْم

سورة المجادلة ، الآية ﴿١١﴾

Supervisors Certification

We certify that this thesis is titled **(High Reflectance Nanolayers Prepared from (Al-Ni-Cr) Alloy for Laser Resonator via Thermal Evaporation Technique)** will be prepared by **(Huda Raad Abdulridha Mohammed)**under our supervisions at Department of Physics, College of Science, University of Babylon, as a partial fulfillment of the requirements for practical work of Physics Master thesis in (Material Physics).

Signature:

Supervisor: Dr. Abdulazeez O. Mousa
Title: Professor
Address: Department of physics - College of Science- University of Babylon

Date: / / 2021

Signature:

Supervisor: Dr.Khalid Haneen Abass
Title: Professor
Address: Department of physics College of Education for pure Sciences- University of Babylon

Date: / / 2021

Certification of the Head of the Department

In view of the available recommendations, I forward latter thesis for debate by the examination committee.

Signature:

Name:Dr. Abdulazeez O. Mousa
Title: Professor
Address: Head of Physics Department / College of Science / University of Babylon
Date: / /2021

Dedications

First and foremost this humble work is dedicated to Almighty God

to fill me with strength and power

To my father, Cindy

To my loving mom for her patience and constant support, And care.

To my brothers and sisters

To my honorable supervisors

HUDA

Acknowledgments

I should thank my Almighty (Allah) for helping me in completing my thesis.

I would like to express my deep thanks and gratitude to my supervisors,

Prof.Dr. Abdulazeez O. Mousa Al-Ogaili and prof.Dr.Khalid Haneen Abass *for remarkable notes during the whole work of mine.*

Many thanks to Department of Physics, College of Science, University of Babylon. and Department of Physics ,College of Education for Pure Sciences for offering me the opportunity to complete my thesis .

HUDA

Summary

In this study, (Al-Ni-Cr) alloy nano-layers with various thicknesses (1-layer (90 nm), 1-layer (25 nm), 2-layers (40 nm), 3-layers (65 nm)), were prepared by thermal evaporation technique on glass substrates under pressure of 10^{-7} mbar. It was observed through the results that the structure of these films were amorphous and there is no direction of the films. No peaks appear refer to so fine crystal structure from (XRD) test and surface of the (Al-Ni-Cr) alloy thin films are homogeneous, smooth, totally coated, and free from defects such as pin holes and cracks. The beans are distributed in the same size, dense, well defined.

It was observed that the small spherical granules distributed over the substrate surface and it was found that the size of these grains increased with increasing thickness. Only nanocrystalline grains were observed, and the surface shapes were virtually unchanged, regardless of sedimentation time ,therefore it is difficult to obtain SEM images due to the small grain sizea from (SEM and AFM)tests. The optical properties of (Al-Ni-Cr) alloy thin films were mainly studied by recording transmittance spectra with a UV-Visible spectrophotometer in the range of (200-1100)nm. From these spectra, it observed a decreasing in the transmittance with increase wavelength. In general, that with increasing film thickness the permeability decreases.

This behavior is due to the increase in the number of atoms of the thickness, that leads to increase the number of collisions between incident photon and atoms, which lead to the increasing of absorbance and decreasing transmittance . The results can comparable with that of reflectance. the transmittance decreases with increasing thickness, while the reflectivity of nanofilms examine using 635 nm and 532 nm laser wavelength . The reflectance reached to 98% for t_1(90nm) and t_4(65nm) for

635 nm and 99% for the wavelength of 532 nm. The results refer to possibility to use these films in the reflective coatings such as laser resonator and fibers.

The dispersion parameters were calculated using the Wemple–DiDomenico process. The single oscillator energy of electronic transition (E_o) and the dispersion energy (E_d) both reduced as layer thickness increased. Reflective and executed films have very small energy gap values. The electrical properties of the (Al-Ni-Cr)nano films were primarily investigated through conductivity measurements. This shows that the (Al-Ni-Cr) nano films behave as a conductor. It's noticed from the study of electrical properties (electrical resistivity), (Al-Ni-Cr) nanofilms may be suitable to fabricate electrical circuits with high conductivity.

Contents

List of Figures

List of Tables

List of Symbols and Abbreviations

Symbol	Description
SWS	Spatial Wavefunction-Switched
L.R.O	Long Range Order
S.R.O	Short Range Order
FWHM	Full Width at Half Maximum
θ	Bragg Diffraction Angle
D_s	Debye Scherrer's
a	The Lattice Constants
S	The Micro Strains
δ_D	The Dislocation Density
N_ℓ	The Number of Crystallite Layer
n_i	Intrinsic Carrier Concentration

Symbol	Description
J	Current Density
σ	Electrical Conductivity
E	Electric Field
μ_d	Carrier Mobility
n-type	Concentration of Electrons
p- type	Concentration of Holes
V.B	Valence Band
C.B	Conductive Band
XRD	X-Ray Diffraction
M.P	Melting Point
AFM	Atomic Force Microscope
SEM	Scanning Electron Microscope
UHV	Ultra High Vacuum
E_g	Energy Gap
λ_c	The Cutoff Wavelength
T	Transmittance
R	Reflectance
A	Absorption
$h\upsilon$	Photon Energy
k_o	Extinction Coefficient
α	Absorption Coefficient
λ	Wavelength
A_o	Constant Involving The Properties of The Bands
r	Constant Depending on The Nature of The Transition
E_p	Energy of Phonon Assisting in The Indirect Transition

Symbol	Description
n_o	Real Part of Complex Refractive Index
n	Refractive Index
E_u	Urbach Energy
I_0	Photon Beam of Intensity
I_t	Intensity of Light Transmitted
c	Speed of Light in Vacuum
v	Speed of Light in Medium
R	Resistance
L	Length
V_H	Hall Voltage
RT	Room Temperature
B	Magnetic Field
μ_n	Electron Mobility
μ_P	Hole Mobility
μ	Mobility
P_g	The Total Resistivity
ρ_1	Grain Resistivity
ρ_2	The Grain Boundaries Resistivity
t	Thickness
I	Electric Current
σ_p	Hole Conductivity
$\sigma_{optical}$	Optical Conductivity
q	Charge of Electron
m	Evaporated Mass of Materials
d	Distance between Source (Boat) and Substrate

Symbol	Description
ρ	Evaporated Density of Materials
ΔX	Shift Between the Interference Fringes
X	The Distance Between the Interference Fringes
CRDS	Cavity Ring Down Spectroscopy
HR	Highly Reflective
WDD	Wemple–DiDomenico
E_o	The Energy of the Effective Single Oscillator
E_d	The Dispersion Energy
TGA	Thermo Gravimetric Analysis
Kp	Equilibrium Constant
S_Z	Ten Point Height
RMS	Root Mean Square

1.1 General Introduction

Special properties such as light weight, high strength and economic value must refer to products usually used in the aviation industry, car and ship. In modern metallography the Al-Ni-Cr alloys are particularly attractive, given their greater mechanical properties, especially at high temperature rates, steepness and a combination of high hardness and high corrosion resistance [1]. The aluminum alloys used to cover the surface oxide of aluminum and chromium have a broader use in connection with the formation. This film has protective coating proprieties which can be regenerated following mechanical damage [2]. Although the small amount of aluminium in the Al-Ni-Cr alloy system studied since the 1950s, just a few recent researches were devoted to its high-Al [3]. These alloys used as layers in interconnect within a semiconductor devices, the nickel or chromium contents are no greater than 0.5 weight percent. The low concentration of nickel and chromium makes the layer close to the other aluminum-based layers possible for deposition and design [4].

The development of nanoparticulate-containing thin films will lead to new uses for photonics, catalytics, electronics, magnetism and biometrics[5]. Despite recent progress in creating diverse type of functional nanoparticles [6-8], the development of conformal thin, physicochemical property-controlled nanopartikel films remains a challenge. Anti-reflection (AR) filters were commonly used in various applications as glass telescopes, lenses, mirrors, solar cells, IR diodes, large- narrow-band filters, auto and architectural glass, and displays including cathode ray tubes and screens plasma, and flat panels. Also, dielectric mirrors were inhanced for use in gas lasers and interferometers of Fabry-Perot [9]. A number of the techniques based on top-down lithography have been used to produce antireflectant spatial wavefunction-switched (SWS) on Si surfaces, such as the photolithograph[10], electron-beam

lithography [11], lithography for laser interference[12], and nanoimprint [13]. In this work, we study the structure and examine the high reflectance nanolayers prepared from Al-Ni-Cr alloy by thermal evaporation technique.

1.2 Nanomaterials

Nanomaterials are the particles (crystalline or amorphous) of organic or inorganic materials having sizes in the range of (1-100) nm. Nanomaterials are classified into nanostructured materials and nanophase materials. The former refer to condensed bulk materials that are made of grains with grain sizes in the nanometer size range while the latter are usually the dispersive nanoparticles [14].

Nanomaterials can be nanoscale in one dimension (surface films), two dimensions (strands or fibres), or three dimensions (particles).They can exist in single, fused, aggregated or agglomerated forms with spherical, tubular, and irregular shapes. Common types of nanomaterials include nanotubes, quantum dots and fullerenes.

The classification of nanomaterials is based on the number of dimensions, which are in nano range (≤ 100 nm)[14], as shown in figure (1.1)[15]:

a- 0D nanomaterials have all the dimension within nanoscale, i.e. no dimension is larger than 100 nm. The most common example of 0D- dimensional nanomaterials is the nanoparticle. These nanoparticles can be crystalline or amorphous, metallic, ceramic, or polymeric.

b- 1D nanomaterials have at least one dimension in nano range. This leads to needle like shaped materials having one dimension at nanoscale.1D nanomaterials include nanoplatelets, nanorods, nanoclays and nanosheets.

c- 2D nanomaterials have two dimensions in nano range. 2D nanomaterials include nanofibers, nanotubes, nanorods and whiskers. Carbon nanotubes are good example of 2D nanomaterials.

d- 3D nanomaterials have all three dimension in nano range. 3D nanomaterials include nanogranules, nanoclays and equiaxed nanoparticles.

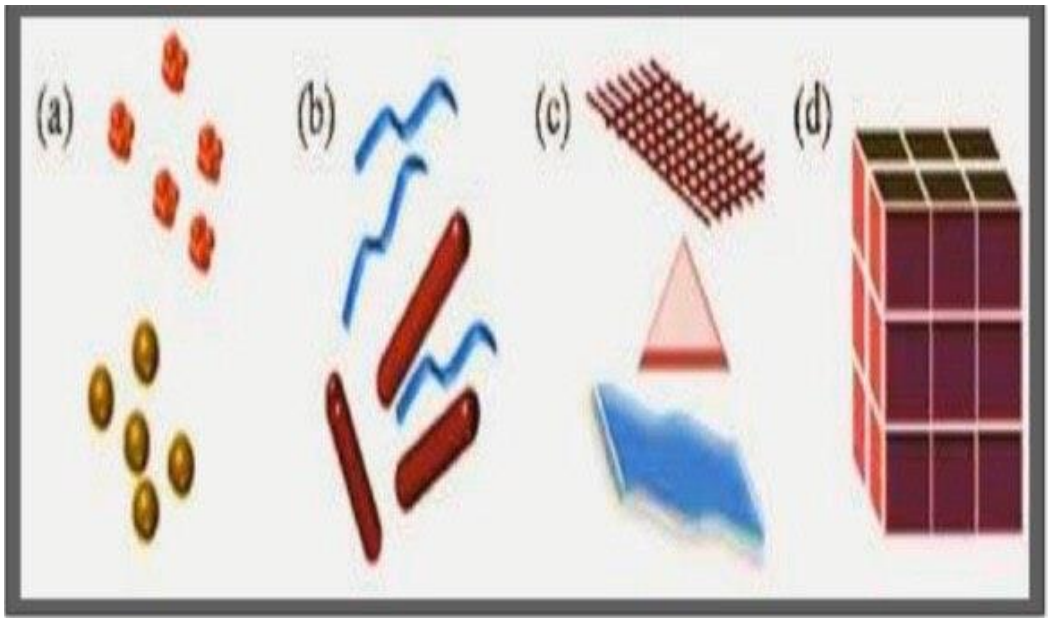

Fig.(1.1): Classification of Nanomaterials (a) 0D nanomaterials; (b) 1D nanomaterials; (c) 2D nanomaterials; (d) 3D nanomaterials[15].

The nanomaterials can be crystalline or amorphous or polycrystalline. They can composed of a single or multi-phase chemical elements. They could be in various forms and shapes, metallic, ceramic or polymeric.There are many different ways of creating nanostructures, macromolecules or nanoparticles or buckyballs or nanotubes and so on can be synthesized artificially for certain specific materials[14].

1.3 Synthesis of Nanomaterials Methods

In general, top-down and bottom-up are the two main approaches for nanomaterials synthesis[16].

a. Top-down: size reduction from bulk materials.

b. Bottom-up: material synthesis from atomic level.

Top-down routes are included in the typical solid –state processing of the materials. This route is based with the bulk material and makes it smaller, thus breaking up larger particles by the use of physical processes like crushing, milling or grinding. Usually this route is not suitable for preparing uniformly shaped materials, and it is very difficult to realize very small particles even with high energy consumption[16].

The biggest problem with top-down approach is the imperfection of the surface structure. Such imperfection would have a significant impact on physical properties and surface chemistry of nanostructures and nanomaterials. It is well known that the conventional top-down technique can cause significant crystallographic damage to the processed patterns[17].

Bottom –up approach refers to the build-up of a material from the bottom: atom-by-atom, molecule-by-molecule or cluster-by-cluster. This route is more often used for preparing most of the nano-scale materials with the ability to generate a uniform size, shape and distribution. It effectively covers chemical synthesis and precisely controlled the reaction to inhibit further particle growth. Although the bottom-up approach is nothing new, it plays an important role in the fabrication and processing of nanostructures and nanomaterials.Synthesis of nanoparticles to have a better control over particles size distribution, morphology, purity, quantity and quality, by

employing environment friendly economical processes has always been a challenge for the researchers. The choice of synthesis technique can be a key factor in determining the effectiveness of the photovoltaic as studies. There are many methods of synthesizing titanium dioxide, such as hydrothermal, combustion synthesis, gas-phase methods, microwave synthesis and sol-gel processing. This research focuses on sol- gel processing and characterization techniques which was discussed in great detail[18].

1.4 Thin Film Deposition Methods

Based on the nature of deposition process the methods employed for thin film deposition can be broadly classified into two groups i.e. physical and chemical methods [19]. All possible deposition processes are shown in Figure (1.2). In physical methods the film material is moved from a target source with some form of energy to the substrate. This technique is widely used in one-component films, like metal films. Under physical methods, we have vacuum evaporation and sputtering, where the deposition takes place after the material to be deposited has been transferred to a gaseous state either by evaporation or an impact process. Chemical film fabrication methods involve chemical reactions and the precursors are mostly components undergoing reaction at the substrate surface or in the vicinity of the substrate. Under chemical methods, we have the gas phase chemical processes and solution techniques [20].In this work we used evaporation method.

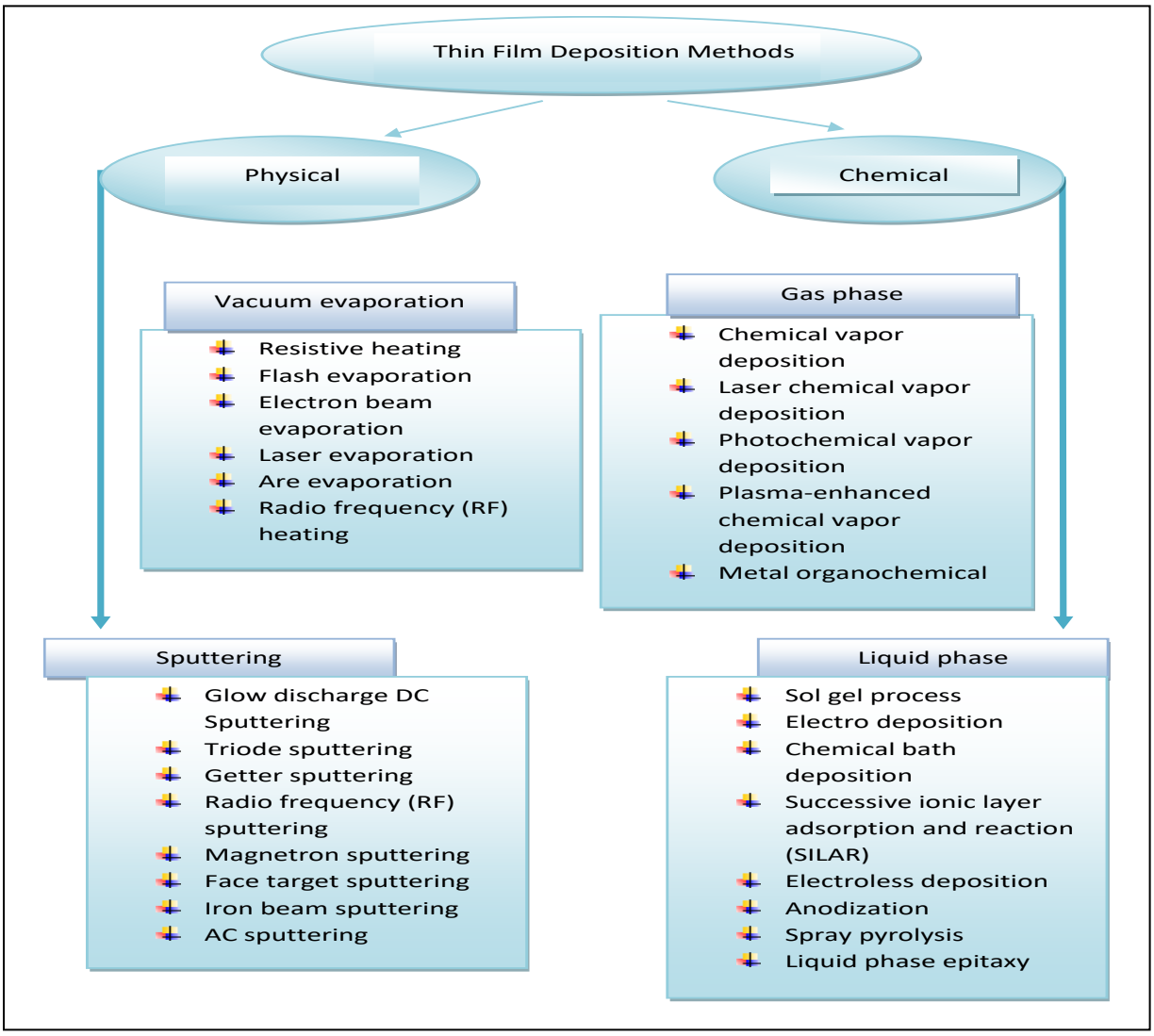

Fig. (1.2): Classification of Thin Film Deposition Processes Physical and Chemical Methods[20].

1.5 Characterization of (Al-Ni-Cr) Alloy

Pure aluminum is soft and hardness limited, therefore, the manufacturers are usually made of aluminum alloys with small amount of copper, zinc, and other elements such as nickel and chromium. Alloys of the aluminum-nickel-chromium (Al-Ni-Cr) alloy attract great attention in the modern metallography, because of its high mechanical properties at high temperature especially yielding, stiffness and

combine high hardness with high resistance for corrosion [21]. Coating used aluminum alloys have wider applications connection with the formation on surface oxide film of aluminum and chromium. This film provides protective coating properties able to regenerate after mechanical damages [22].

Many of our modern technologies require materials with unusual combinations of properties that cannot be met by the conventional metal alloys, ceramics, and polymeric materials. This is especially true for materials that are needed for aerospace, underwater, and transportion applications. For example, aircraft engineers are increasingly searching for structural materials that have low densities, are strong, stiff, and abrasion and impact resistant, and are not easily corroded [23].

The aluminum alloys having two very important features, the first one, low density and the second corrosion resistance, for these reasons, these alloys are used widely in aircraft industry and motors [24].

The interest in thin films raised from the wide range of use and applications in electronic equipments and devices such as transistors, detectors, solar cells, etc. This leads to the study of electronic and optical properties of thin films. Nanostructured materials have been attracted a great deal of attention in the last few years for their unique characteristics which are not obtained from conventional macroscopic materials. Owing to quantum size effects and surface effects, nanoparticles can display novel optical, electronic, magnetic, chemical, and structural properties that might find many important technological applications. An extremely active and prolific field in nanomaterials find ways to control size and morphology of the nanoparticles since the properties and applications of the nanoparticles are largely dependent on their size and morphology [25].

1.6 Literature Survey

This section includes previous studies by researchers and the results of their work:

In (2010) W.Kowalski, ***et al***., [26] studied a contribution to the (Al–Pd–Cr) phase diagram. they found five ternary structures were revealed in a quite small compositional range adjusting to that of the Al–Cr μ-phase. One, resembling the high-temperature Al_3Mn phase (T-phase, orth. a = 1.47, b = 1.24 and c = 1.25 nm), is formed in a small region around $Al_{77}Pd_7Cr_{16}$ composition. A hexagonal structure with a = 1.77 and c = 1.25 nm resembling Al–Ni(Cu)–Cr μ-phase was revealed around $Al_{81.5}Pd_{1.5}Cr_{17}$ and another hexagonal structure with very close lattice parameters around $Al_{73}Pd_{11}Cr_{16}$. A ternary ϵ-phase resembling that in Al–Ni–Cr (orth., a = 1.24, b = 3.46 and c = 2.04 nm) was found at 970 °C around the $Al_{77.5}Pd_{1.5}Cr_{21}$ composition. An additional orthorhombic phase with a = 2.48, b = 3.87 and c = 2.04 nm was found to be formed between about $Al_{80}Pd_4Cr_{16}$, $Al_{73}Pd_8Cr_{19}$, $Al_{77}Pd_4Cr_{19}$ and $Al_{77}Pd_6Cr_{17}$. Partial 930, 970, 990 and 1020 °C isothermal sections are presented.

In (2011) M. Gojic, ***et al***.,[27] studied electrochemical and microstructural of (Cu–Al–Ni) shape memory alloy. The corrosive behaviour of (Cu–Al–Ni) shape memory alloy in deaerated 0.5 M NaCl solution at 20 °C was studied by means of open circuit potential measurements, linear polarization, potentiodynamic polarization measurements, cyclic voltammetry and electrochemical impedance spectroscopy measurements. The results of impedance measurements at open circuit potential have shown that the overall impedance of the system increases with immersion time due to continuous growth of the passive film on the alloy surface. The XRD and EDX analysis showed the presence of copper, aluminium and nickel compounds, Cu-oxides and Cu-chlorides on alloy surface.

In (2012) K. H. Abass, [28] studied prepared (Al-Ni-Cr) alloy ingots contain (0.25, 0.5, 0.99) and 1.98 at.% Ni-Cr. He prepared nanofilms with thicknesses (8, 15, 25) nm from Al-Ni-Cr alloys that deposited by thermal evaporation technique under vacuum of 10^{-5} mbar onto glass substrate at a temperature of 298 K and rate of deposition 0.2 nm/sec. Also he studied morphological and optical properties of these nanofilms. The measured transmittance values decrease with increasing both of Ni-Cr content and thickness with the range of 90-94% at 8 nm. From the alloy the optical band gaps of the alloy decrease with increasing both of Ni-Cr content and thickness with the values (2.3, 2.27, 2.25, 2.3 and 2.1) eV, (1.55, 1.5, 1.45, 1.35 and 1.3) eV, and (1.5, 1.45, 1.4, 1.3 and 1.2) eV for samples at thicknesses 8nm, 15nm, and 25nm, respectively.

In (2013) Z. Sun, ***et al***.,[29] studied new design aspects of creep-resistant NiAl-strengthened ferritic alloys. Ferritic alloys strengthened with NiAl precipitates are being developedfor elevated-temperature applications. Due to the high concentration of Al in these alloys, they feature a relatively low density of ∼7 g cm^{-3}. In this paper, the high-temperature mechanical behavior of NiAl-strengthened ferritic alloys is reviewed. Further, they discuss another related class of alloys, where the precipitate strengthening is provided by Ni_2TiAl-type precipitates rather than NiAl. These relatively unexplored alloys may enhance the creep resistance of precipitate-strengthened ferritic alloys.

In (2014) C. M. Chang, ***et al***.,[30] studied Al–Ni–Y–X (X = C u, Ta, Zr) metallic glass composite thin films for broad-band uniform reflectivity. They found that the relationship among composition, atomic structure and reflectivity performanceis established. Compared with pure Al films, the (Al–Ni–Y) film surface roughness is much lower and hardness is much higher, more suitable for optical reflector applications. For composite (Al–Ni–Y) films, the reflectance varies within (80–

91)%. For fully amorphous films, the reflectivity exhibits unusual uniform reflection at~70%, perfect for broad-band reflector.

In (2015) K. H Abass and Sh. L. Hamdan, [31] studied effect of thickness on the optical properties of (Al-Ni-Cr) thin films prepared by thermal evaporation technique. Al-Ni-Cr thin films with different thickness (18, 26, and 30) nm were prepared by thermal evaporation technique on glass substrates under vacuum of10^{-7} mbar. The influences of the thickness on the optical properties of (Al-Ni-Cr)alloy thin films were mainly investigated from recording the absorbance and transmittance spectra by UV-Visible spectrophotometer in the range of (200- 1100) nm. From these spectra, the transmittance decreased with increasing of thickness, while the absorbance increased with increasing of thickness. The values of optical energy gap decreases from (1.8 to 0.73) eV when thickness increased from(18 to 30) nm. The optical conductivity increased with increasing thickness.

In (2016) V.G.Shmorgun, ***et al***.,[32]studied effect of the high-heating on the chemical and phase composition of the (Al-Ni-Cr) layered coatings. The transformation of the structure, phase and chemical composition of the diffusion coatings of the system Al-Ni and (Al-Cr-Ni) at 1100 °C is studied. It is shown that the diffusion redistribution of Al by the coating thickness during the heat treatment is slower in the system (Al-Cr- Ni) than in the binary system Al-Ni.

In (2017) P.Pandey, ***et al***.,[33]studied development of high-strength high-temperature cast (Al-Ni-Cr) alloys through evolution of a novel composite eutectic structure. Aiming to develop high-strength Al-based alloys with high material index (strength/density) for structural application, this article reports a new class of multiphase Al alloys in the (Al-Ni-Cr) system that possess impressive room temperature and elevated temperature (200 °C) mechanical properties. The ternary eutectic and near eutectic alloys display a complex microstructure containing

intermetallic phases displaying hierarchically arranged plate and rod morphologies that exhibit extraordinary mechanical properties.

In (2018) M.Kawamura, ***et al.***, [34]studied metal nanolayer deposited highly stable Ag thin films and their optical properties they had reported that deposition of several-nm-thick Al surface layer on Ag thin films improved thermal stability remarkably. They investigated the influence of the deposition of Al nanolayer on the reflectance of the Al/Ag multilayer. 100-nm-thick Ag film and (1–5)nm thick Al surface layer were deposited successively by vacuum evaporation, and their optical properties were measured. the samples on which a 5-nm-thick Al layer was deposited on the Ag film showed decreased reflectance.

In (2019) K.M.Oluwasegun, ***et al***.,[35]studied hot corrosion of Ni-Cr alloys.The hot corrosion behavior of three nickel base alloys were investigated in fused salts (Na_2SO_4 - 10 wt% NaCl) environment. The oxidation kinetics, scale morphologies, phases and porosity are measured by thermo gravimetric analysis (TGA), Field electron microscopy (FE-SEM), EDS and image analyzer respectively. In addition to FE-SEM analysis, microstructure of the samples are seen by optical microscope. Susceptibility to hot corrosion was found to be correlated to the scale formed during oxidation.

In (2020) T. Stefanova, ***et al.***, [36]studied thin film metallic glass broad-spectrum mirror coatings for space telescope applications. The use of metallic glasses as coatings on silicon carbide substrates for applications as optical mirrors was investigated. Various alloy compositions were chosen, limited by the available method of synthesis by electric arc melting, using the rule of mixtures to predict their reflectance. After a preliminary experimental study on bulk specimens, two alloys were selected for production as thin film metallic glasses by physical vapour deposition on silicon carbide substrates. The alloy $Zr_{44}Cu_{40}Al_8Ag_8$ (at.%) was sputtered

from a single target. In a separate co-sputtering experiment, two targets, one of $Al_{90}Ni_5Y_5$ (at.%), the other of pure Zr, were deposited. The structure, roughness, and reflectance of the films were investigated. The measured reflection was compared with the predicted values for wavelengths between 250 nm and 2000 nm. The reflectance of the Al-based mirrors was uniform around 70% across the UV/Vis/near-IR spectrum range significantly improving that of the polished silicon carbide substrate.

In (2021) D. Aryanto, ***et al***.,[37] studied microstructure and oxidation behavior of an Al–Ni–Cr–Cu–MoO_3–SiO_2 composite coating on low-carbon steel. In the present study, an Al–Ni–Cr–Cu–MoO_3–SiO_2 composite coating with varying elemental compositions was deposited using the mechanical alloying technique. The composite coating had a thickness in the range of (36–59) μm, with good and continuous adherence to the substrate. The cyclic oxidation curve of the composite coating followed a parabolic rate law. The sample that contained 5.3 wt% MoO_3 showed the best oxidation resistance after 10 oxidation cycles at 800 °C. This sample had a lower mass gain than the other samples. Moreover, this sample had a Kp of 1.2×10^{-3} mg^2/cm^2. Protective Al_2O_3 oxides formed on the composite coating surface with a thickness of (0.75–1.89) μm. This oxide scale was dense and fully adhered to the coating, thereby improving oxidation resistance.

1.7 Aim of the Work

The aim of this work can be listed as following:

1- Preparation of nanofilm layers of (Al-Ni-Cr) alloy with different thicknesses, by thermal evaporation technique on glass substrates under pressure of 10^{-7} mbar .

2- To obtain thin films that fully reflect the applications of the laser resonator. And when it is adopted as the main membrane,will get good electrical conductivity that can be adopted in the manufacture of electrical circuits with high conductivity.

2.1 Introduction

This chapter covers on a general description of the theoretical parts measurements; structural, optical, electrical for Al-Ni-Cr thin films. Finally, this chapter gives a theoretical review including all the relations, scientific explanations, and the equations which are used in this thesis.

2.2 Basic Theory of Characterization Techniques of Thin Film

In the last years ,the advancement in science has taken place mainly with the discovery of new materials. Characterization is an important step in the development of exotic materials. The complete characterization of any material consists of phase analysis, compositional, structural, and surface characterization, which have strong bearing on the properties of materials. In this section different analytical technique used to characterize our thin films are described.

2.2.1 Structural and Morphological Characterization

A wide variety of characterization techniques were used to evaluate the material quality of the thin films before using the films in applications. The structural properties of the films were studied by X- ray diffraction (XRD). The morphology of surface thin films was studied by atomic force microscopy (AFM) and scanning electron microscopy (SEM).

2.2.1.1 Basic Theory of X-ray Diffraction (XRD)

X-ray diffraction (XRD) is a powerful technique for determination the crystal structure and lattice parameters. The basic principles of X-ray diffraction are found in textbooks e.g. by Fox [38]. A basic instrument for such study is the Bragg spectrometer [39]. The relationship describing the angle at which a beam of X-rays of a particular wavelength diffracts from a crystalline surface was discovered by William H. Bragg and W. Lawrence Bragg and is known as Bragg's law [40].

$$2d_{(hkl)}sin\theta = m\lambda \qquad (2\text{-}1)$$

Where, (λ) is wavelength of the X-ray, (θ) is Bragg diffraction angle of the XRD peak in degree (scattering angle), (m) is integer representing the order of the diffraction peak, and $(d_{(hkl)})$ is inter-plane distance of (i.e atoms or ions or molecules). The crystallite size of the deposits is estimated from the full width at half maximum (FWHM) of the most intense diffraction line by Debye Scherrer's formula as follows [41].

$$D_S = \frac{0.94\,\lambda}{\beta\,cos\,\theta} \qquad (2\text{-}2)$$

Where, D_S is crystallite size, and β is (FWHM) in radians. The X- ray diffraction data can also be used to determine the dimension of the unit cell. The lattice constants (a) and (c) of the wurtzite structure for thin film can be calculated as given below [42].

$$a = \frac{2}{\sqrt{3}}\, d_{(hkl)} \qquad (2\text{-}3)$$

and

$$c = 2d_{(hkl)} \qquad (2\text{-}4)$$

The micro strains value (S) are caused during the growth of thin films, and will be raised from stretching or compression in the lattice to make a deviation in the c-lattice constant of the hexagonal structure [43]. This micro strain can be calculated from the relation [44].

$$S = \frac{\beta\,cos\,\theta}{4} \qquad (2\text{-}5)$$

The dislocation density (δ_D) is a measure of the number of dislocations in a unit volume of a crystalline material, and can be evaluated by relation [45]:

$$\delta_D = \frac{1}{D_S^2} \qquad (2\text{-}6)$$

For thin films the microstructural factor like film texture may be considered as the powerful means that control electrical properties of polycrystalline film

materials[46] . The number of crystallite layer (N_ℓ) which could be calculated due to the percolation theory, and it depends on the film thickness (t) as the relation [47]:

$$N_\ell = \frac{t}{{D_s}^2} \qquad (2\text{-}7)$$

2.2.1.2 Basic Theory of Atomic Force Microscope (AFM)

The atomic force microscopy AFM show in figure(2.1) is a mechanical imaging instrument that measures the three dimensional topography as well as physical properties of a surface with a sharpened probe. The sharpened probe is positioned close enough to the surface such that it can interact with the force fields associated with the surface. Then the probe is scanned across the surface such that the forces between the probe remain constant [48]. An image of the surface is then reconstructed by monitoring the precise motion of the probe as it is scanned over the surface. Typically the probe is scanned in a raster-like pattern. AFM analyses in order to find the average grain size and surface topography at atomic scale of the samples [49].

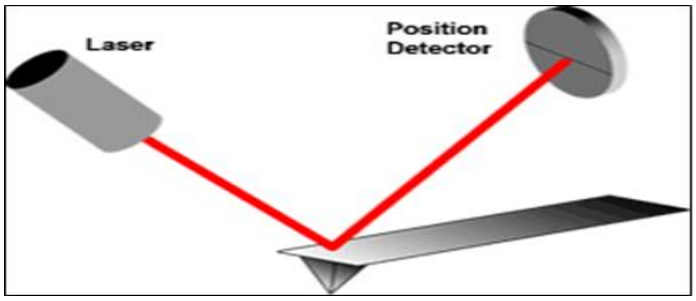

Fig.(2.1): Beam Deflection System, Using a Laser and Photodetector to Measure the Beam Position[49].

2.2.1.3 Basic Theory of Scanning Electron Microscope (SEM)

A more recent and extremely useful investigative tool is the scanning electron microscope (SEM) show in Figure(2.2). The surface of a spacemen to be examined is scanned with an electron beam, and the reflected (or back-scattered) beam of

electrons is collected, and then displayed at the same scanning rate on a cathode ray tube. The image on the screen, which may be photographed, represents the surface features of the sample. The surface may or may not be polished and etched, but it must be electrically conductive a very thin metallic surface coating must be applied to nonconductive materials. Magnifications ranging from 10 to in excess of 50000 times are possible, as are also very great depths of fields. Accessory equipment permits qualitative and semi quantitative analyses of the elemental composition of very localized surface area [50].

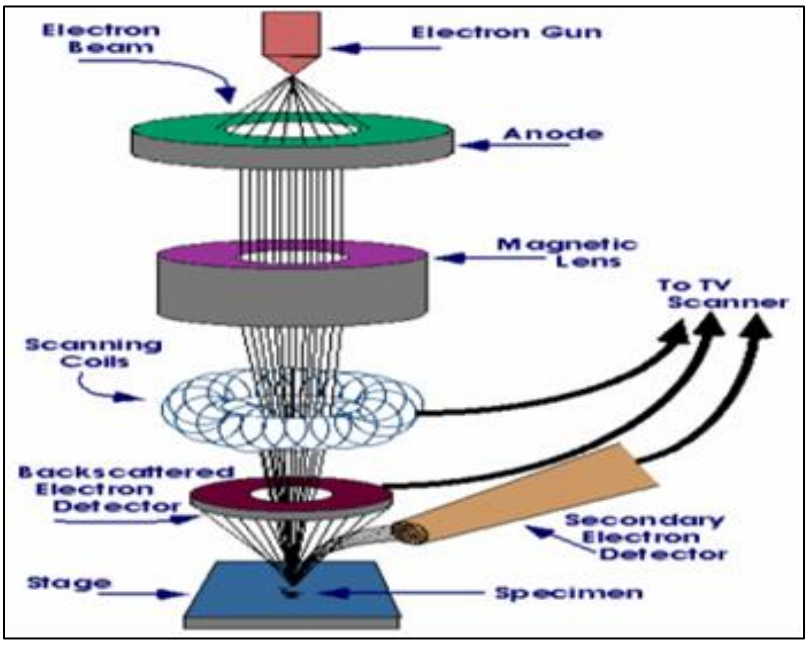

Fig. (2.2): Set-up Illustrates the SEM [50].

2.2.2 Optical Characterization

The study of the optical properties of a material is interesting for many reasons. Firstly, the use of materials in optical applications such as interference filters, optical fibers, and reflective coating requires accurate knowledge of their optical constants over a wide range of wavelengths. Secondly, the optical properties of all materials may be related to their atomic structure, electronic band structure and electrical properties.

2.2.2.1 Reflectivity

Reflectivity can be obtained from absorption and transmission spectrum in accordance to the law of conservation of energy by the relation [51]:

$$R + \mathrm{T} + \mathrm{A} = 1 \qquad (2\text{-}8)$$

Where:

R: is the reflectivity, T: is the transmittance and A:is the absorbance.

2.2.2.2 Optical Absorbance and Transmittance

An important technique for measuring the band gap of material is the absorption of incident photons by the material. The main absorption process in semiconductors and dielectric originates form the interaction of light with electrons [52]. If the photon has a frequency such that its energy matches the energy needed to excite an electron to a higher allowed state, then the photon may be absorbed. If the energy of the incoming photon does not match the required excitation energy, no excitation occurs and the material is transparent to such radiation [53].

If a beam of photons with $h\upsilon \geq E_g$ falls on a material, there will be some predictable amount of absorption, determined by the properties of the material. We would expect the ratio of transmitted to incident light intensity depend on the photon wavelength and the thickness of the sample. To calculate this dependence, assume that a photon beam of intensity (I_o) is directed at a sample of thickness (t). The beam pass through the sample has intensity (I) at a distance (x) from the surface, its can be calculated by considering the probability of absorption within any increment (dx). Thus, the degradation of the intensity –dI/dx is proportional to the intensity remaining at (x) [54].

$$-\frac{dI}{dx} = \alpha I \qquad (2\text{-}9)$$

The solution of this equation is [54]:

$$I = I_o e^{-\alpha x} \qquad (2\text{-}10)$$

and the intensity of light transmitted through the sample thickness (t) is

$$I_t = I_o e^{-\alpha t} \qquad (2\text{-}11)$$

Where the coefficient (α) is called the absorption coefficient.

The cutoff wavelength (λ_c) is the fundamental absorption edge, which is related to the optical energy gap by the following relation [55]:

$$\lambda_c = \frac{1240}{E_g} \qquad (2\text{-}12)$$

Where:

E_g: Energy gap (eV)

λ_c: Cutoff wavelength (μm)

2.2.3 Electrical Properties

The measurement of resistivity is on the whole straight forward; by measuring the resistance (R) of semiconductor bar of known length (L), and uniform known area (A, as given in equation) [56]:

$$\rho = \frac{RA}{L} \qquad (2\text{-}13)$$

The resistivity is defined as the proportionality constant between the electric field (E) and the current density. Electrical resistivity is the reciprocal of electrical conductivity as shown in the following equation [57].

$$\sigma = \frac{1}{\rho} \qquad (2\text{-}14)$$

For semiconductors with both electron and holes the resistivity is[57] :

$$\rho = \frac{1}{\sigma} = \frac{1}{q\,(\mu_n n + \mu_P p)} \qquad (2\text{-}15)$$

Where :

μ_n: electron mobility, and μ_p: hole mobility.

The resistivity of a semiconductor is an important in device design. In polycrystalline semiconductor, the conductions are complicated because of the existence of grain and grain boundaries and its effect on transport process, and charge carriers inside the material. Petrilz suggests in accordance to existence of grains the total resistivity [58].

$$\rho_g = \rho_1 + \rho_2 \qquad (2\text{-}16)$$

Where ρ_1 represents grain resistivity and ρ_2 is the grain boundaries resistivity. Orten and Powell improved this theory for polycrystalline and suggest a model for electrical conduction in these materials [59].

2.3 Thermal Evaporation

A thermal evaporator uses an electric resistance heater to melt the material and raise its vapor pressure to a useful range. This is done in a high vacuum, both to allow the vapor to reach the substrate without reacting or scattering against other gas-phase atoms in the chamber, and reduce the incorporation of impurities from the residual gas in the vacuum chamber [60,61]. Thermal evaporation is the simplest way of depositing material onto a substrate under pressure $1 \times 10^{-7}\ mbar$ and given excellent purity of films. Figure (2.3) explains the configuration of a basic coating system [62,63].

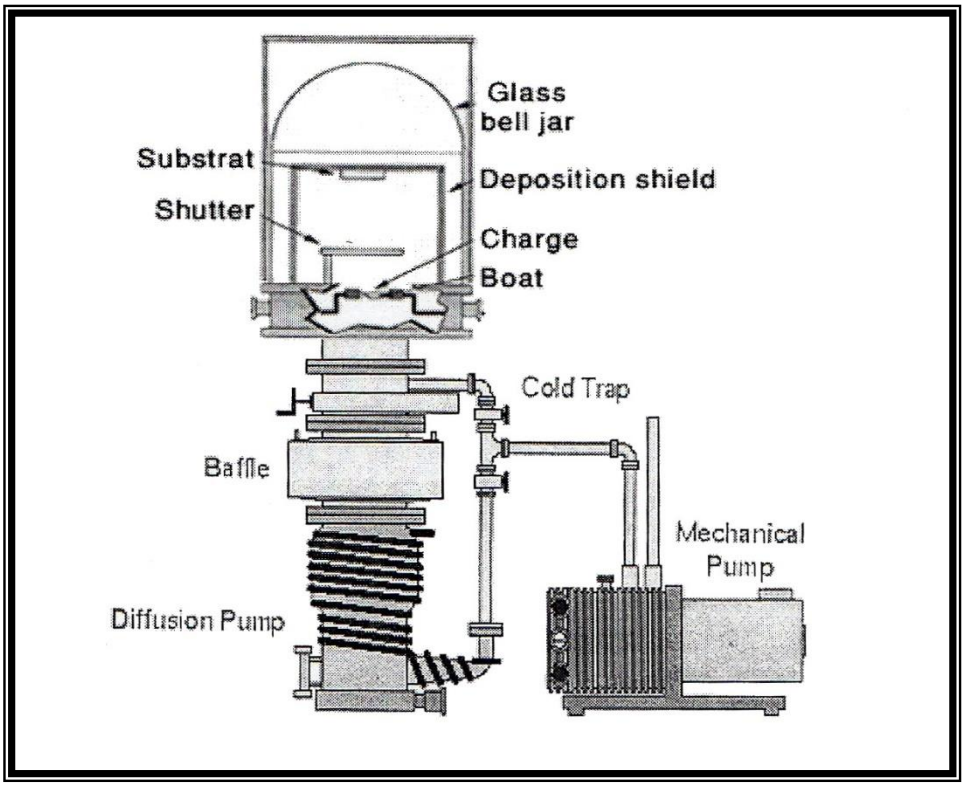

Fig. (2.3): Configuration of a Basic Coating System [63].

2.4 Thickness Measurement

Thickness is one of the most important thin film parameters since it largely determines the properties of the film. The thickness of the films is usually measured by monitoring the rate of the deposition during the coating process. Two methods have been approved to measure the thickness of thin film, first it is necessary to estimate the amount that must be evaporated to get the thickness of the film required called the weighted method and the second is optical. Vacuum deposited films used for structural, electrical, optical or other purposes must normally be deposited to a specified thickness.

The weighting method was used in this study. This method determines the required amount of evaporated material which was used to give desired thickness using the following equation [64].

$$t=m/2\rho\pi R^2 \qquad (2\text{-}17)$$

Where :

t=is the film thickness in (cm)

m =is the mass of the materials to be evaporated in (g)

d = is the source (boat) to substrate distance

ρ = is the density of materials to be evaporated

R = is the distance between the substrate and the boat (cm)

This method gives an estimate of the deposited films thickness that is safe to work. The error percentage in this method is 20%.

Film thickness measurements by optical interferometer method have been obtained. This method is based on interference of the light beam reflection from thin film surface and substrate bottom, with error rate at 3%. The film thickness (t) is given by [64]:

$$t = \frac{\lambda}{2}.\frac{\Delta X}{X} \qquad (2\text{-}18)$$

Where ΔX is the shift between the interference fringes, X is the distance between the interference fringes, and λ is the He:Ne wavelength (6328Å).

2.5 The Materials Conductivity

Solid-state materials, according to their conductivities, can be classified into three classes: conductors, semiconductors, and insulators. At room temperature, the conductor has conductivities between (10^8-10^3) $\Omega^{-1}cm^{-1}$, semiconductor between (10^3-10^{-8}) Ω^{-1} cm^{-1}, and insulator between (10^{-8}-10^{-18}) Ω^{-1} cm^{-1} [65].According to the

atomic arrangement of solid, the materials can be divided into three types known as crystalline, polycrystalline and non-crystalline (or amorphous) solids [66].

In crystalline solid, the atoms or molecules have a regular geometric arrangement or periodicity. These solids have a high degree of ordering, and thus have long range order (L.R.O.) in three dimensions, as shown in Figure (2.4.a).

The polycrystalline materials have a high degree of ordering over many small regions. These regions are called grains and they are separated from one and another by grain boundaries. These materials are characterized by short range order (S.R.O.) as shown in Fig.(2.4.b). The amorphous materials have ordering only within a few atomic or molecular, as shown in Fig.(2.4.c).

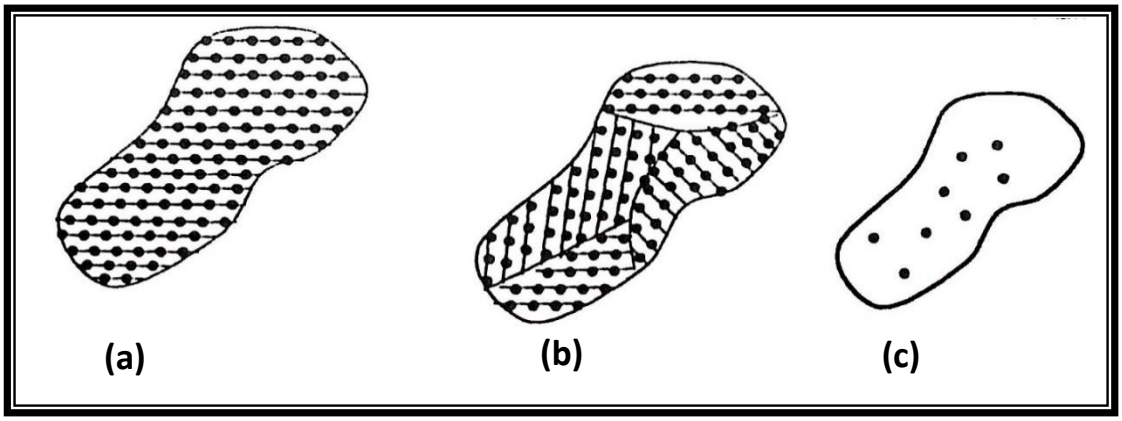

Fig.(2.4): Schematics of Three General Types of Solids[66]:
a) Crystalline, b) Polycrystalline and c) Non crystalline (amorphous).

The most important characteristics of the semiconductors which distinguish them from metals and insulators are the negative temperature coefficient of resistivity and the existence of energy gap [67].

Semiconductors are in general element such as germanium (Ge), Silicon (Si), carbon (C), and Tin (Sn). According to the pureness of the semiconductors, a perfect one of them which contains no impurities or crystal defects is called intrinsic

semiconductors. In such material, there are no free charge carriers at absolute zero temperature, but as the temperature rises, electron-hole is generated. In this type of semiconductors, the conduction can be carried out by the electrons and holes. The concentration "n" of electrons in the conduction band (C.B) equals to the concentration "p" of holes in the valence band (V.B), and then we have[68]:

$$n = p = n_i \qquad (2\text{-}19)$$

Where n_i is the intrinsic carrier concentration.

In addition, the current density "J" is given by:

$$J = \sigma E \qquad (2\text{-}20)$$

Where σ is the electrical conductivity and E is the electric field.

The charge concentration in a semiconductor can be rapidly increased by introducing appropriate impurities into the crystal lattice by a process called doping [69]. In this process, only one type of carrier is predominant, either electrons or holes and hence produces either n-type semiconductor and the semiconductor material is known as "extrinsic".

The conductivity in the case of extrinsic (n-type) semiconductors is given by:

$$\sigma = ne\ \mu_d \qquad (2\text{-}21)$$

Where (μ_d) is known as the carrier drift mobility.

2.6 Highly Reflective (HR) Coatings

Highly reflective (HR) coatings are used to minimize loss while reflecting lasers and other light sources. Absorption and scatter during reflection lead to decreased throughput and potential laser-induced damage. HR coatings are used in common laser optics applications such as folding a laser's beam path and laser cavity end

mirrors. Metallic mirror coatings are used to create reflective components for many applications but laser applications tend to require a higher reflectivity than those offered from standard metallic mirror coatings. Because of this, multilayer dielectric HR coatings are usually used for laser mirrors instead of metallic mirror coatings, as they can achieve higher reflectivity. Metallic surfaces reflect light because loosely attached electrons freely oscillate with incident light waves without much impedance or hindrance, but all metals will absorb some amount of incident light. This makes metallic mirror coatings susceptible to damage when used with high power lasers[70].

Dielectric HR coatings reflect light based on constructive interference during Fresnel reflections and have the complete opposite purpose of AR coatings in that they utilize constructive interference to maximize Fresnel reflections instead of utilizing destructive interference to minimize them Figure (2.5). The constructive interference is caused by alternating layers of a high and low refractive index materials with thicknesses specifically chosen to maximize reflectivity at a given wavelength range. In a λ/4 dielectric mirror, also known as a Bragg mirror, the thickness of each layer corresponds to a quarter of the design wavelength.Layer thickness is based on the wavelength in the material, not the vacuum wavelength[71].

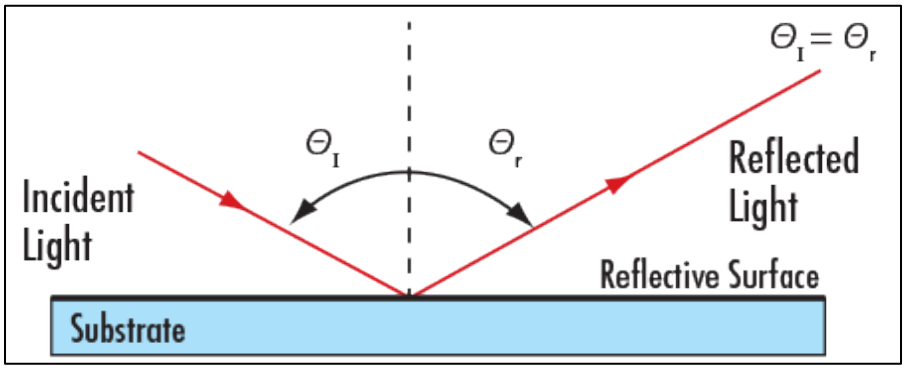

Fig.(2.5): Reflection from a Surface Mirror.[71]

High reflectivity mirrors, with reflectivity ranging from 99.8% up to 99.999%, are essential components in most laser systems for beam steering while maximizing throughput. It is common industry practice to determine mirror reflectivity by measuring transmission using spectrophotometry and assuming that the rest of the light was reflected. However, this false assumption does not consider scatter or absorption, leading to overly optimistic reflectivity values. For mirrors with reflectivities above 99.5%, a more accurate way to determine reflectivity is to measure total loss through cavity ring down spectroscopy (CRDS)[72].

2.7 Dispersion Energy Parameters

Energy dispersion parameters have an important role in identifying the characteristics of the optical material. As through them one can calculate the necessary factors required to design the optical communication and the spectral dispersion devices.Wemple–DiDomenico (WDD) single effective oscillator Model successfully describes the dispersion of the refractive index [73-75]. This model has an advantage in fitting the experimental data because it provides an intuitive physical interpretation of the measured quantities [76]. The main outputs of this model are the energy of the effective single oscillator E_o and the dispersion energy E_d.

The energy E_o or sometimes called average energy gap gives quantitative information on the overall band structure of the material. It must be taken into consideration that, the information obtained from E_o is completely different from those obtained from the optical energy gap E_g. Optical energy gap is related to the optical properties near the fundamental absorption edge of the material. In spite of the difference between E_o and E_g , yet there is an approximate empirical equation

showing that the oscillator energy, E_o is often twice the optical energy gap , E_g i.e. ($E_o \approx 2E_g$) [75].

On the other hand, the dispersion energy E_d, which represents oscillator strength, measures the average energy of interband optical transitions and is associated with adjustment in the structural order of the sample i.e., it is related to the ionicity, anion valency and coordi- nation number of the material. It is worth to mention here that, the dis- persion energy, E_d is very nearly independent on the effective single oscillator energy E_o. This is because E_d is proportional to the dielec- tric loss, while E_o does not rely on the dielectric loss, either close or from afar. According to (WDD) model, the relationship between (E_o, E_d) and the incident photon energy (hυ) is given as follows [73,74]:

$$(n^2 - 1) = \frac{E_d\, E_0}{{E_0}^2 - (h\nu)^2} \qquad (2\text{-}22)$$

Where:

n: refractive index

E_o: the energy of the effective single oscillator

E_d : the dispersion energy

hυ :incident photon energy

The moments of optical spectra (M_{-1} and M_{-3}) can be calculate from the next relations [77]:

$$E_0^2 = \frac{M_{-1}}{M_{-3}} \qquad (2\text{-}23)$$

$$E_d^2 = \frac{M^3{}_{-1}}{M_{-3}} \qquad (2\text{-}24)$$

3.1 Introduction

This chapter is dedicated to the experimental part, which plays a significant role in determining the results. It begins with the deposition of (Al-Ni-Cr) alloy thin films layers by using vacuum evaporation method. Then, the optical and electrical measurements are presented.

3.2 Preparation of Thin Films Layers from (Al-Ni-Cr) Alloy

The process of preparing nano-films in several layers includes several stages:

3.2.1 Materials

The Al-Ni-Cr alloy was prepared by the researcher [78]. Al-Ni-Cr alloys were prepared by melting together; Aluminum wire, nickel powder and very small pieces of chromium in an electric furance at 800°C under an argon atmosphere after preparing the alloy, heat treatment used for 1300 hours at 560° C [78]. In this work we used (Al-Ni-Cr) alloy of different weights to form films of different thicknesses, where t_1 with a weight of 0.035g, t_2 with a weight of 0.009g, t_3 with a weight of 0.006g two layers, and t_4 with a weight of 0.009g three layers, and the thicknesses t_1 (one-layer (90 nm)),t_2 (one-layer (25 nm)),t_3 (two-layers (40 nm)), and t_4 (three-layers (65 nm)). Where $t_3 = t_1 + t_2$ and $t_4 = t_1 + t_2 + t_1$, as shown in the table (3.1) . A schematic diagram of the experimental work shown in figure (3.1).

Table (3.1): The Prepared Nano Layers of (Al-Ni-Cr) Alloy.

Film symbol	No. of layers	Thickness(nm)
t_1	1	90
t_2	1	25
t_3	2 = t_1+t_2 =25+15	40
t_4	3 = t_1+t_2+t_1 =25+15+25	65

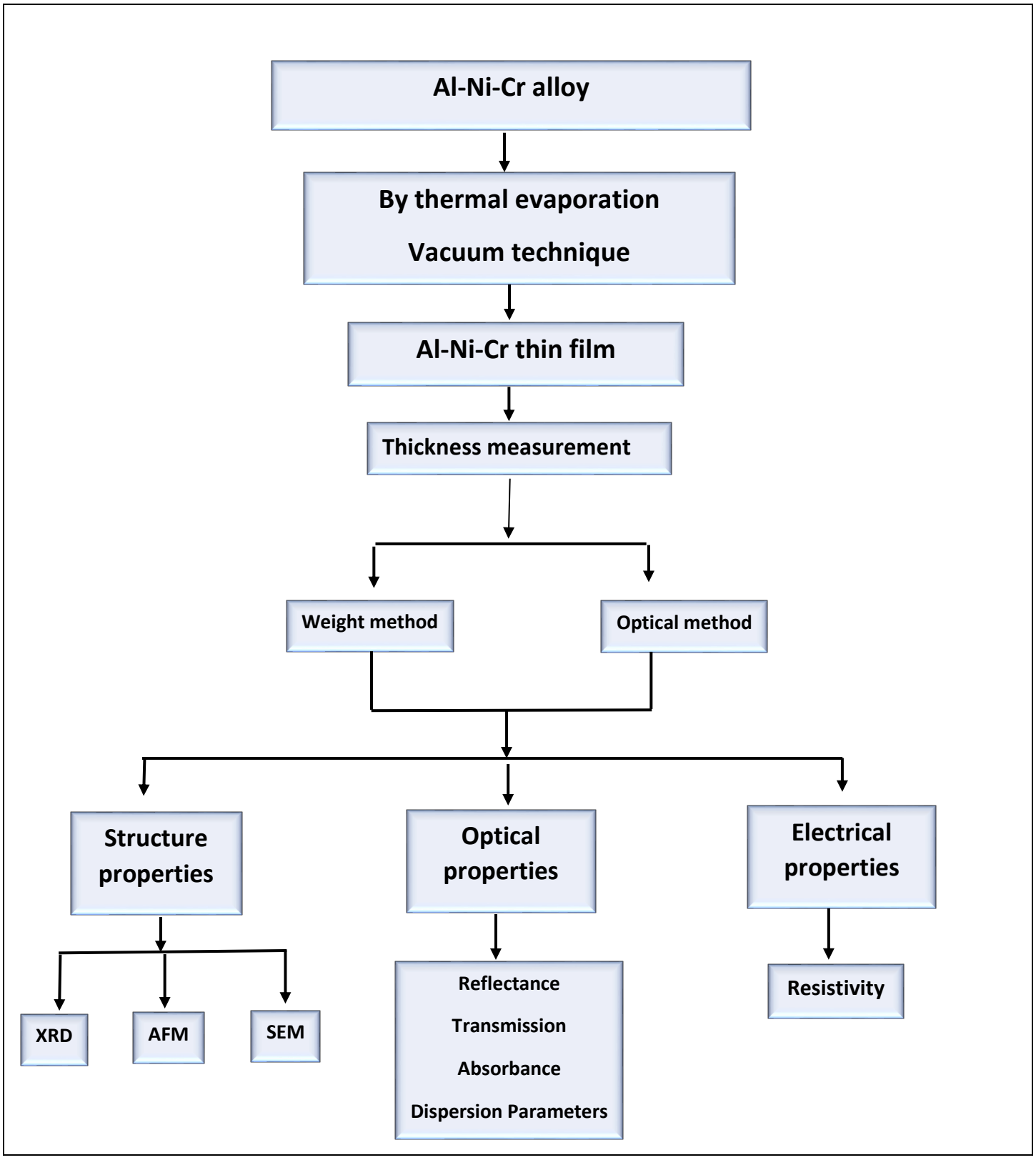

Fig.(3.1): Schematic Diagram of Experimental work.

3.2.2 Substrate Preparation

Type and nature of the substrate are the influence parameters and have the most important effects on the properties of the deposited films. One type of substrates were used in this study, glass slides which were used to study the structural, electrical and optical properties of Al-Ni-Cr thin films.First step glass slides and cleaning, the substrate used for deposits Al-Ni-Cr thin films in this work is a microscopic glass slides. These glass slides substrates (8 × 2.5) cm^2 with 1 mm thickness were subjected to the following steps:

1- The substrates were cleaned by water and a detergent solution to remove any oil or dust that might be on their surface.
2- The substrates were immersed in a clean beaker containing distilled water.
3- The distilled water was replaced by pure alcohol or pure acetone and the previous step was repeated.

Finally the glass substrates were dried by an air-jet and were wiped with soft paper.

3.3 The Specification of Boat

Various types of sources were used for the evaporation. A spiral boat source of tungsten material were used for the (Al) evaporation to make electrodes, and molybdenum boat source is used for the deposition of (Al-Ni-Cr) thin films as shown in figure (3.2).

Fig. (3.2): (a) Spiral Tungsten Boat and (b) Molybdenum Boat.

3.4 The Coating Unit

The vacuum unit system, Edwards coating unit model Edwards-c has been used for the deposition of Al-Ni-Cr thin films. The main constructions of the typical vacuum coating unit are shown in Figure(3.3).

Fig. (3.3): Thermal Evaporation System.

The system is pumped down to a vacuum of 10^{-7} mbar, an electric current was passed through the boat gradually to avoid breaking the boat. When the boat temperature reached the required temperature the deposition process starts with constant rate of deposition equal to 0.5 nm/s. After these steps, the current supply was switched off and the samples were left in the high vacuum, and

then the air was entered to the chamber, and the films were taken out from the coating unit and kept in the vacuum desiccator until the measurements were made. All the samples were prepared under constant conditions (pressure, substrate temperature and rate of deposition); the main parameters that control the nature of the film properties are thickness (90, 25, 40 and 65) nm. In this work the evaporation processes have been performed at room temperature (RT) and the distance between the source and substrate was kept at (15) cm. This system is found in college of education for pure sciences department of physics university of Babylon.

3.5 Thin Film Growth

In the present work, thin films layers of (Al-Ni-Cr) alloy have been obtained by the (Al-Ni-Cr) alloy powder and, the deposition of (Al-Ni-Cr) alloy thin films have been performed by electrical resistance heated thermal evaporation process. In this process, the electrical power is passed through the boat to create a vapor which travels in straight line paths to the substrate. In general, there are three steps in any vacuum deposition process, creation of an evaporant from the source material, transport of the evaporant from the source to the substrate and condensation of the evaporant on to the substrate to form the thin film deposited as in Figure (3.4). In this work, the evaporation processes have been performed at room temperature (RT). The pressure during the evaporation was approximated to $10^{-7}\ mbar$ with a rate of deposition $0.5\ nm.s^{-1}$. The distance between the source and substrate was kept at $15\ cm$.

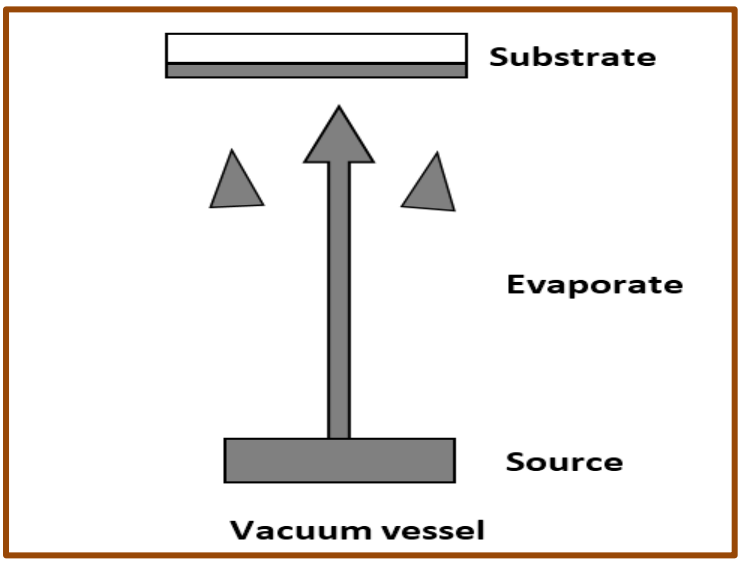

Fig. (3.4): Basic Steps Deposition Processes.

3.6 Preparation of Masks

Various shapes of thick aluminum (Al) foil masks are used on glass substrates to make a suitable shape design for both film and electrodes for the electrical measurements for films deposited at different conditions. Aluminum electrodes were deposited on the surface of (Al-Ni-Cr) thin films using thermal evaporation equipment through a mask giving active area of (0.2×0.2) cm^2 as illustrated in Figure(3.5).

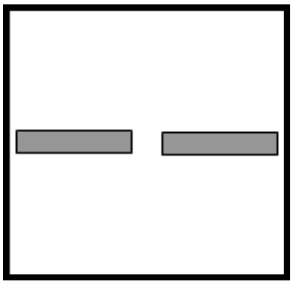

Fig. (3.5): The Mask Used Deposition of Electrodes of DC.

3.7 Thickness Measurement

Thickness is one of the most important thin film parameters. There are several methods used for measuring the thickness of thin film. In this work, the thickness of the films were measured by using the optical measurement and weight method.

1- Weighting Method.

Thickness of the thin films has been calculated according to the following equation [64]:

$$t = \frac{m}{2\pi\rho R^2} \qquad (3.1)$$

Where (t) is thickness of the thin films (nm), (m) is a mass of the material in (g), (ρ) is the density of material (g/cm^3) and (R) is the distance between the substrate and the boat (cm). This method gives an approximate thickness because some of the material lost or fleeing on the sides of the heater.

2- Optical Interferometer Method.

Figure(3.6) shows the photograph of the film thickness measurement, type lambda LIMF-10 , the film thickness was measured with this device in the college of science, university of Babylon.

Fig.(3.6): Image of the Film Thickness Measurement.

3.8 Structural and Morphological Measurements

These measurements include the following

3.8.1 X-ray Diffraction (XRD)

The main purpose of these measurements is to investigate the type of the structure of the prepared thin films. This experimental technique has long been used to determine the overall structure of bulk solids, including lattice constants, identification of unknown materials, orientation of single crystals, orientation of polycrystals, defects, stresses, etc. X-ray diffraction using SHIMADZU X-ray diffracts meter system (XRD – 6000) which records the intensity as a function of Bragg's angle. Samples were examined at the faculty of engineering, university of Babylon, shown in the figure(3.7).

Fig.(3.7) : Image of the XRD

3.8.2 Atomic Force Microscope (AFM)

The surface morphology of the prepared thin films of various thicknesses was observed by AFM type (Aa3000 SPM), shown in the Figure (3.8). Typical data has been taken from AFM height images include root mean square (RMS) roughness and grain size. It has three main modes of mapping topography: contact, intermittent contact (tapping), and non- contact which was used in our-morphology investigation. The most important part of an AFM is the tip with its nanoscale radius of curvature. The tip is attached to a micronscale cantilever which reacts to the Van der Waals interaction and other forces between the tip and sample. The samples were screened

in the laboratories of the college of education for pure sciences in university of Babylon.

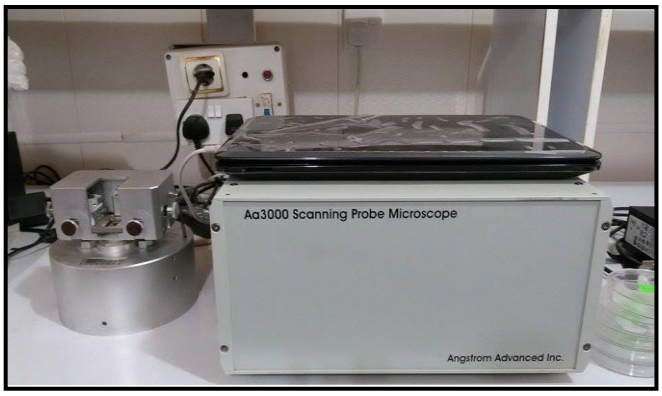

Fig.(3.8): Image of the AFM.

3.8.3 Scanning Electron Microscope (SEM)

Scanning electron microscopy (SEM) is basically a type of electron microscope .The surface morphology of the prepared samples were observed by SEM type (Jeol JSM 6335F), as shown in Figure(3.9). Samples were examined in the faculty of pharmacy, university of Babylon.

Fig.(3.9): Image of the SEM.

3.9 Optical Measurements

The optical absorption spectrum of Al-Ni-Cr thin films layers was recorded in the wavelength range (200-1100) nm using a dual-beam spectrophotometer (UV spectrophotometer shimadzu model UV-1800), as shown in Figure(3.10). The absorption spectrum was recorded at room temperature. The data from the absorption spectrum can be used in computing the optical constants. A computer program was used to obtain transmittance, reflectivity, and absorbance.

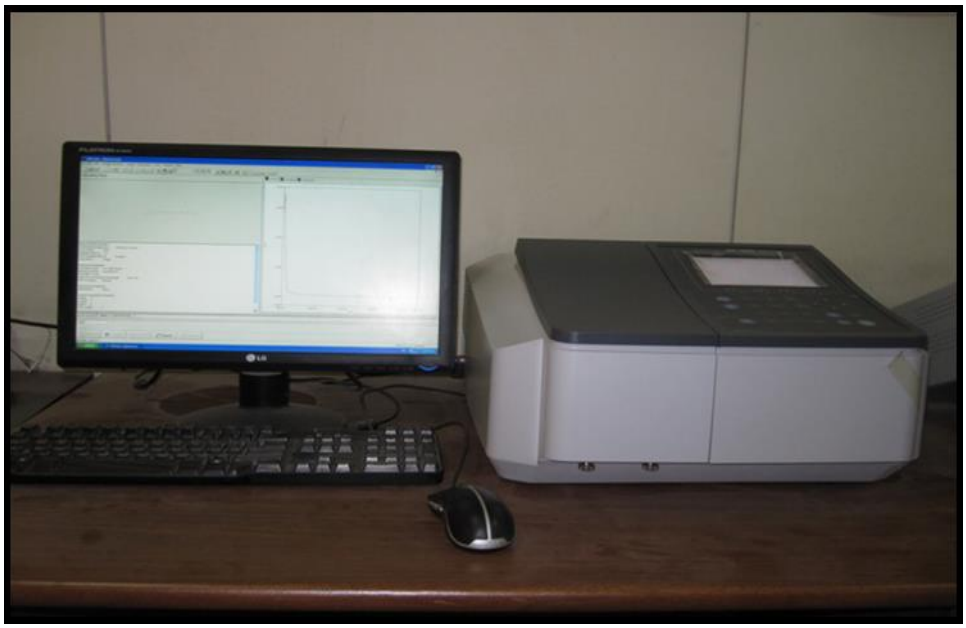

Fig.(3.10): Image of UV-Visible Spectrophotometer.

3.10 Electrical Measurements

The electrical measurements are achieved on prepared thin films including D.C. Electrical conductivity(D.C) of films deposited on glass substrate measured with Al electrodes could be calculated by measuring the D.C electrical resistance using the keithly electrometer (type 2400 source meter) shown in the

figure(3.11), for different temperatures (30-200) °C. The sample was placed in the oven and the electrical resistance was recorded after (5-10) minute to ensure accurate results. The samples were screened in the laboratories of the college of education for pure sciences in university of Babylon.

Fig. (3.11): Image of Keithly Electrometer.

4.1 Introduction

This chapter includes the results and the analysis of the experimental measurements of the (Al-Ni-Cr) nano-layers with various thicknesses , t_1 (one-layer (90 nm)),t_2 (one-layer (25 nm)),t_3 (two-layers (40 nm)), and t_4 (three-layers (65 nm)). Where $t_3 = t_1 + t_2$ and $t_4 = t_1 + t_2 + t_1$ that prepared onto glass substrate by thermal evaporation technique at room temperature (R.T). In addition, study the structural, optical, and electrical properties of prepared nanolayers.

4.2 Microstructural Analysis

In this paragraph several measurements are included:

4.2.1 X-Ray Diffraction Measurements (XRD)

The technique of X-ray diffraction (XRD) was used to know the nature of the crystal structure, the main crystalline stages, and the orientation of the prepared films under certain conditions, as well as to identify some structural variables such as the crystal size. Figure (4.1) represents the (XRD) pattern of the prepared films from (Al-Ni-Cr) alloy.

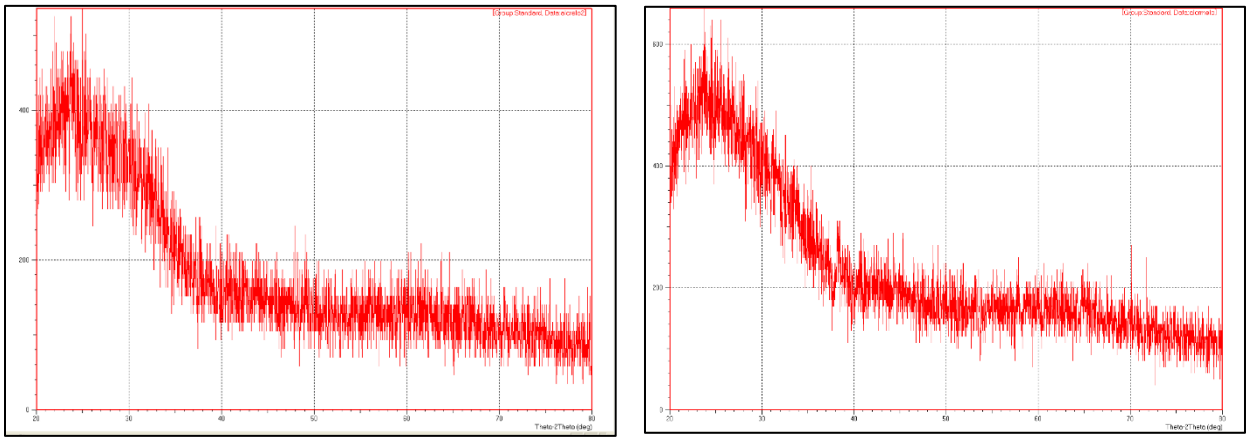

(a) (b)

Fig.(4.1): The X-ray Diffraction Patterns of (Al-Ni-Cr) Nanofilms for a: t_1 (1-layer (90 nm)) and b: t_4 (3-layers (65 nm)).

From Figure (4.1) and through the study of the surface composition of the films, it was observed that the surface of these films was amorphous and there is no direction of the films, no peaks appear to refer to so fine crystal structure. Pictures of (XRD) were taken by the (XRD) device at the university of babylon college of engineering.

4.2.2 Atomic Force Microscope (AFM)

AFM was used to check the film surface. The smoothness of the film surface must be checked. Screening by the morphological study is good evidence of homogeneity. By studying the surface shape, it was observed that the (Al-Ni-Cr) nanofilms of different thicknesses showed that the size of the grains increases with the corresponding increase in the thickness of the prepared films. The (AFM) images of the deposited (Al-Ni-Cr) nanofilms are shown in figures (4.2-4.5), where (a) represents a picture in three dimensions and the highest level was a peak with a rate of (2.29-2.23) nm for the surfaces of these membranes, and (b) represents a picture in two dimensions, and (c) represents the height of the graph of the number of particles, and (d) represents the granular distribution on the surface of these membranes, and (e) represents the graph of the particles.

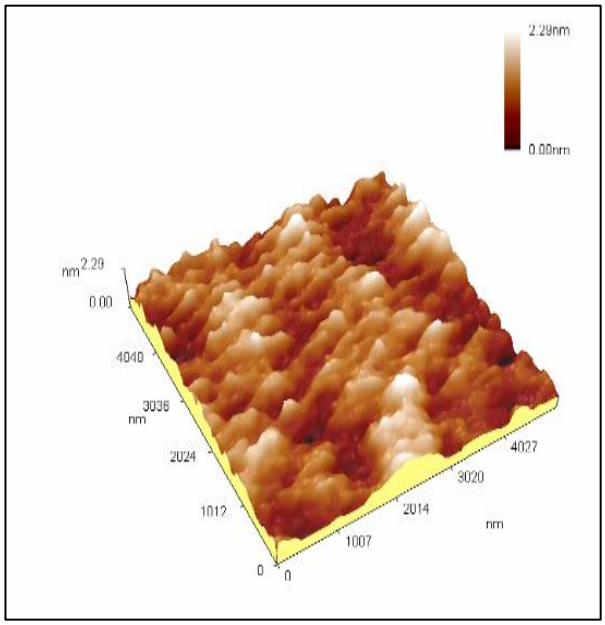

(a)

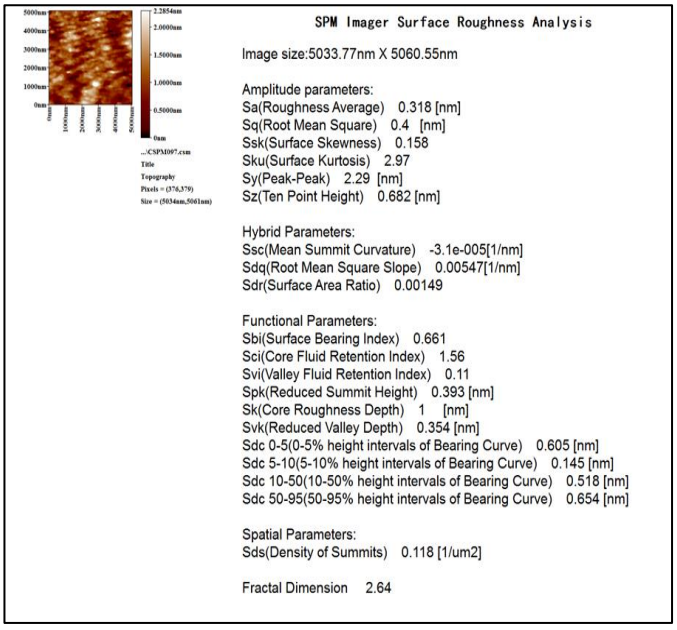

SPM Imager Surface Roughness Analysis

Image size:5033.77nm X 5060.55nm

Amplitude parameters:
Sa(Roughness Average) 0.318 [nm]
Sq(Root Mean Square) 0.4 [nm]
Ssk(Surface Skewness) 0.158
Sku(Surface Kurtosis) 2.97
Sy(Peak-Peak) 2.29 [nm]
Sz(Ten Point Height) 0.682 [nm]

Hybrid Parameters:
Ssc(Mean Summit Curvature) -3.1e-005[1/nm]
Sdq(Root Mean Square Slope) 0.00547[1/nm]
Sdr(Surface Area Ratio) 0.00149

Functional Parameters:
Sbi(Surface Bearing Index) 0.661
Sci(Core Fluid Retention Index) 1.56
Svi(Valley Fluid Retention Index) 0.11
Spk(Reduced Summit Height) 0.393 [nm]
Sk(Core Roughness Depth) 1 [nm]
Svk(Reduced Valley Depth) 0.354 [nm]
Sdc 0-5(0-5% height intervals of Bearing Curve) 0.605 [nm]
Sdc 5-10(5-10% height intervals of Bearing Curve) 0.145 [nm]
Sdc 10-50(10-50% height intervals of Bearing Curve) 0.518 [nm]
Sdc 50-95(50-95% height intervals of Bearing Curve) 0.654 [nm]

Spatial Parameters:
Sds(Density of Summits) 0.118 [1/um2]

Fractal Dimension 2.64

(b)

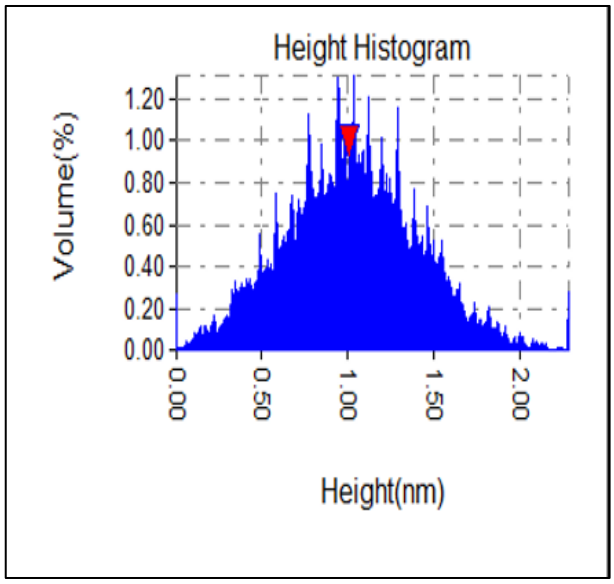

(c)

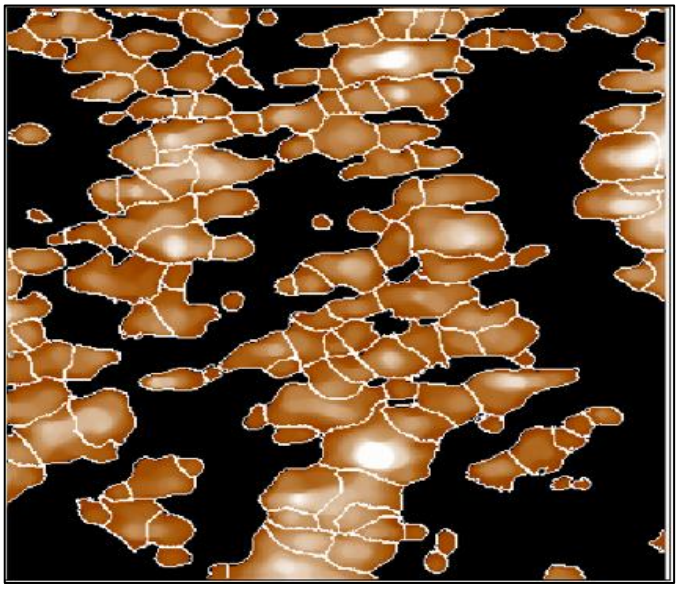

(d)

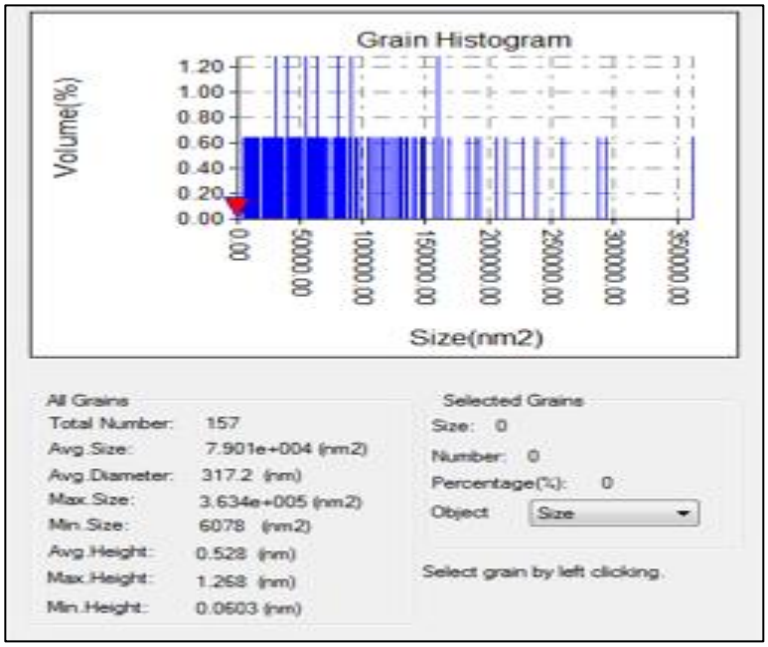

(e)

Fig.(4.2): AFM Image of Al-Ni-Cr Films with Thickness t_1 (1-layer (90 nm)) in a- 3D,b- 2D, c- Height Histogram, d- The Distribution Granular, and e- Grain Histogram.

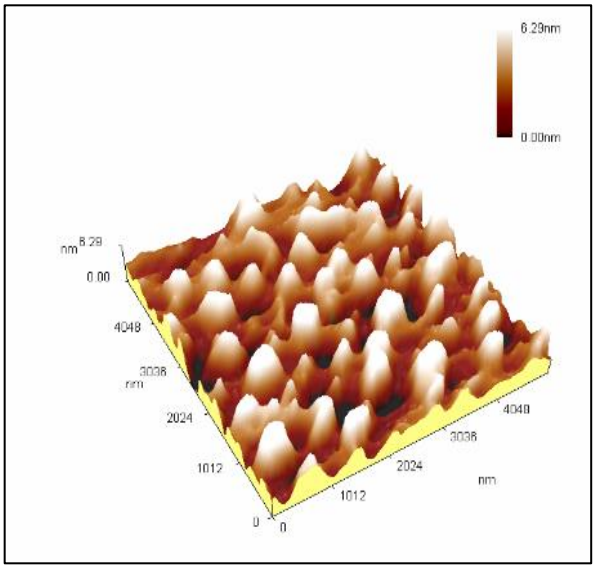
6.29nm
0.00nm
nm 6.29
0.00
4048
3036
2024
1012
0
nm

(a)

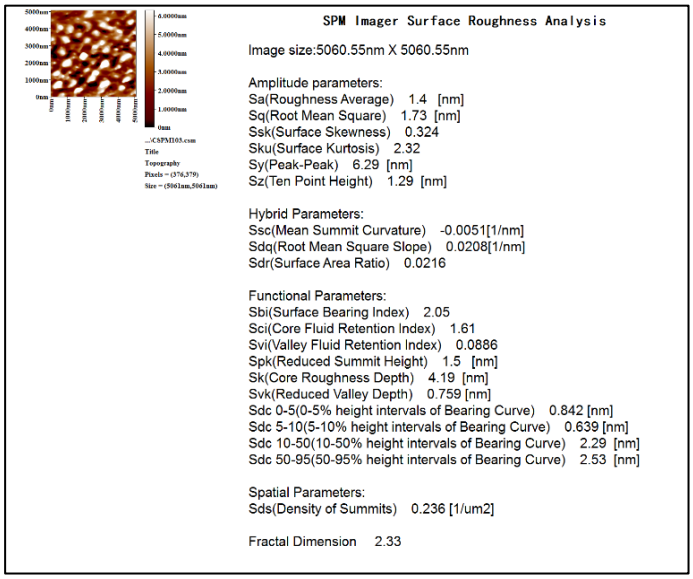
SPM Imager Surface Roughness Analysis
Image size:5060.55nm X 5060.55nm
Amplitude parameters:
Sa(Roughness Average) 1.4 [nm]
Sq(Root Mean Square) 1.73 [nm]
Ssk(Surface Skewness) 0.324
Sku(Surface Kurtosis) 2.32
Sy(Peak-Peak) 6.29 [nm]
Sz(Ten Point Height) 1.29 [nm]
Hybrid Parameters:
Ssc(Mean Summit Curvature) -0.0051[1/nm]
Sdq(Root Mean Square Slope) 0.0208[1/nm]
Sdr(Surface Area Ratio) 0.0216
Functional Parameters:
Sbi(Surface Bearing Index) 2.05
Sci(Core Fluid Retention Index) 1.61
Svi(Valley Fluid Retention Index) 0.0886
Spk(Reduced Summit Height) 1.5 [nm]
Sk(Core Roughness Depth) 4.19 [nm]
Svk(Reduced Valley Depth) 0.759 [nm]
Sdc 0-5(0-5% height intervals of Bearing Curve) 0.842 [nm]
Sdc 5-10(5-10% height intervals of Bearing Curve) 0.639 [nm]
Sdc 10-50(10-50% height intervals of Bearing Curve) 2.29 [nm]
Sdc 50-95(50-95% height intervals of Bearing Curve) 2.53 [nm]
Spatial Parameters:
Sds(Density of Summits) 0.236 [1/um2]
Fractal Dimension 2.33

(b)

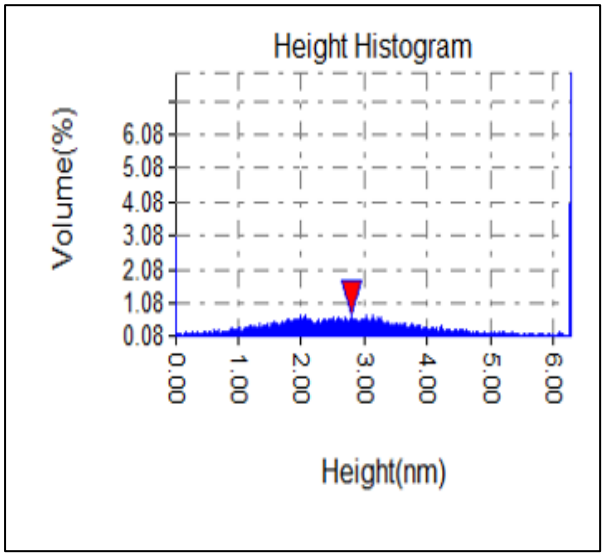
Height Histogram
Volume(%)
6.08
5.08
4.08
3.08
2.08
1.08
0.08
0.00
1.00
2.00
3.00
4.00
5.00
6.00
Height(nm)

(c)

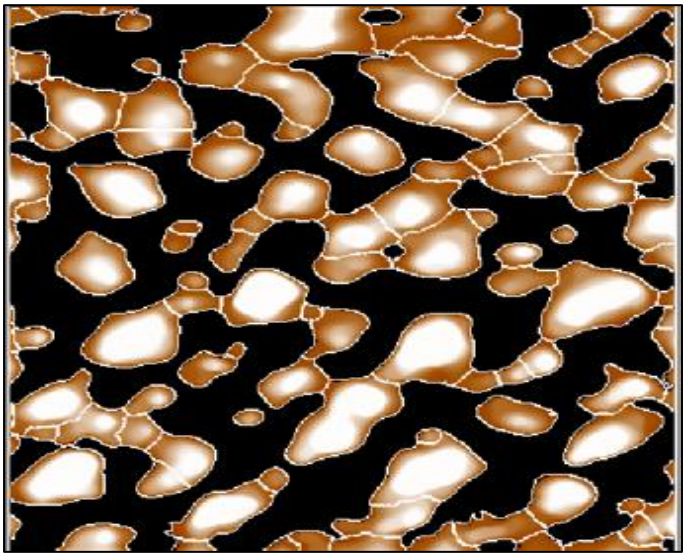

(d)

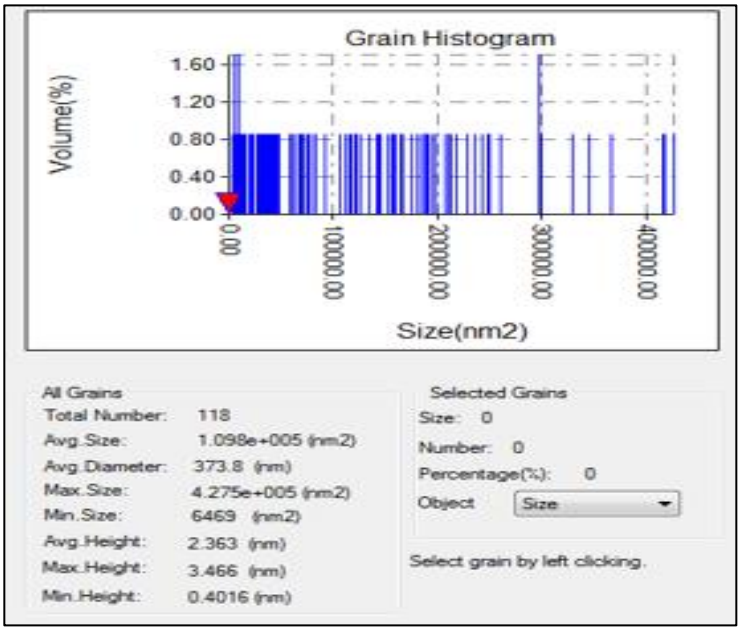

(e)

Fig.(4.3): AFM Image of Al-Ni-Cr Films with Thickness t_2 (1-layer (25 nm)) in a- 3D,b- 2D, c- Height Histogram, d- The Distribution Granular, and e- Grain Histogram.

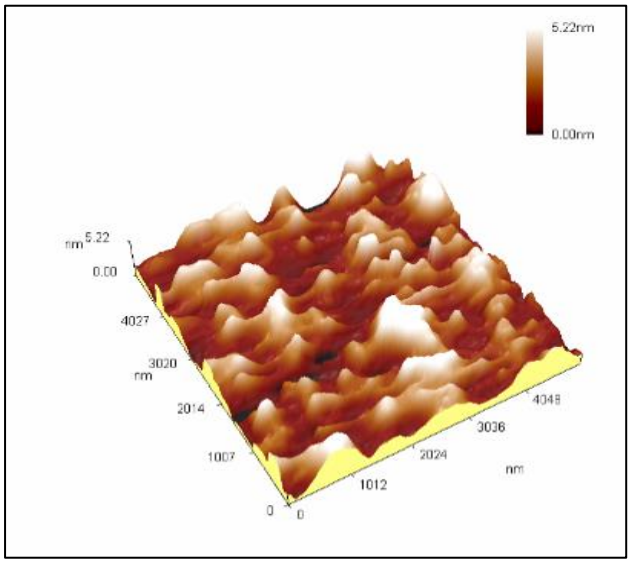
5.22nm
0.00nm
nm 5.22
0.00
4027
3020
nm
2014
1007
0
0
1012
2024
3036
4048
nm

(a)

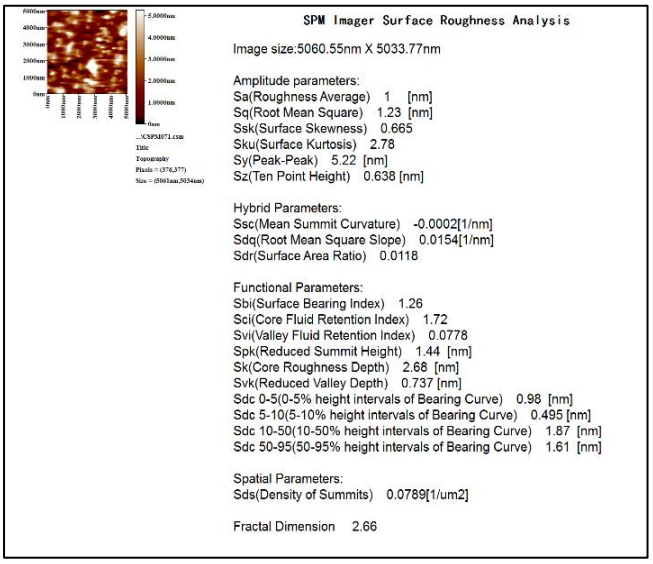
SPM Imager Surface Roughness Analysis
Image size:5060.55nm X 5033.77nm
Amplitude parameters:
Sa(Roughness Average) 1 [nm]
Sq(Root Mean Square) 1.23 [nm]
Ssk(Surface Skewness) 0.665
Sku(Surface Kurtosis) 2.78
Sy(Peak-Peak) 5.22 [nm]
Sz(Ten Point Height) 0.638 [nm]
Hybrid Parameters:
Ssc(Mean Summit Curvature) -0.0002[1/nm]
Sdq(Root Mean Square Slope) 0.0154[1/nm]
Sdr(Surface Area Ratio) 0.0118
Functional Parameters:
Sbi(Surface Bearing Index) 1.26
Sci(Core Fluid Retention Index) 1.72
Svi(Valley Fluid Retention Index) 0.0778
Spk(Reduced Summit Height) 1.44 [nm]
Sk(Core Roughness Depth) 2.68 [nm]
Svk(Reduced Valley Depth) 0.737 [nm]
Sdc 0-5(0-5% height intervals of Bearing Curve) 0.98 [nm]
Sdc 5-10(5-10% height intervals of Bearing Curve) 0.495 [nm]
Sdc 10-50(10-50% height intervals of Bearing Curve) 1.87 [nm]
Sdc 50-95(50-95% height intervals of Bearing Curve) 1.61 [nm]
Spatial Parameters:
Sds(Density of Summits) 0.0789[1/um2]
Fractal Dimension 2.66

(b)

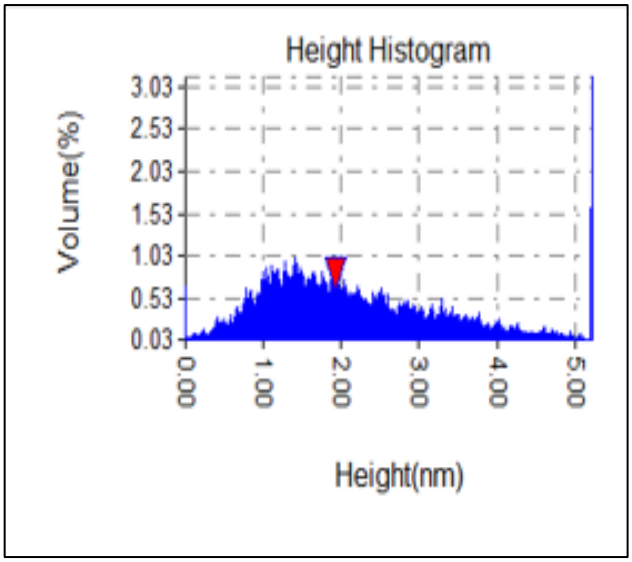
Height Histogram
Volume(%)
3.03
2.53
2.03
1.53
1.03
0.53
0.03
0.00
1.00
2.00
3.00
4.00
5.00
Height(nm)

(c)

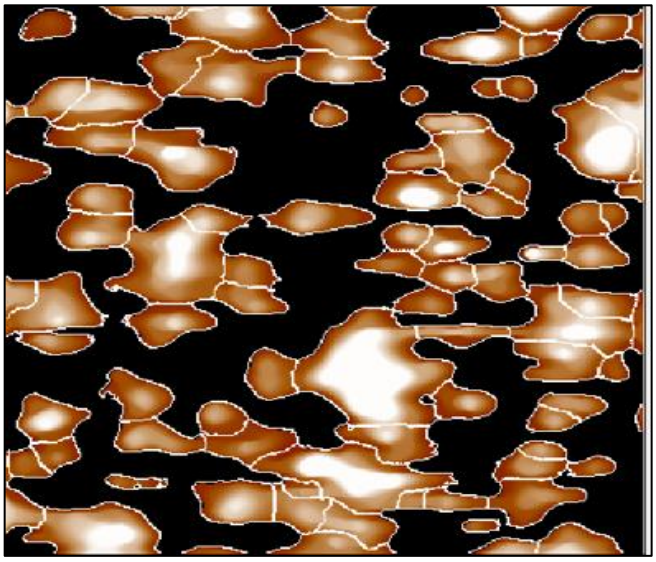

(d)

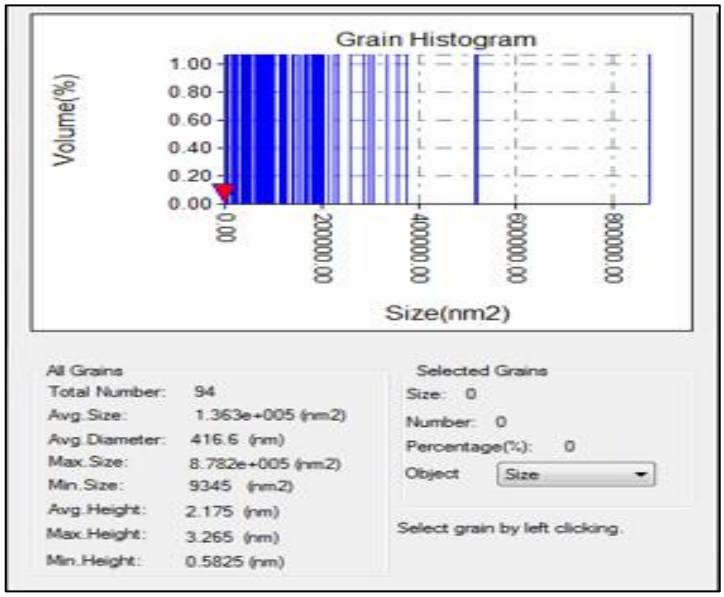

(e)

Fig.(4.4): AFM Image of Al-Ni-Cr Films with Thickness t_3 (2-layer (40 nm)) in a- 3D,b- 2D , c- Height Histogram, d- The Distribution Granular, and e- Grain Histogram.

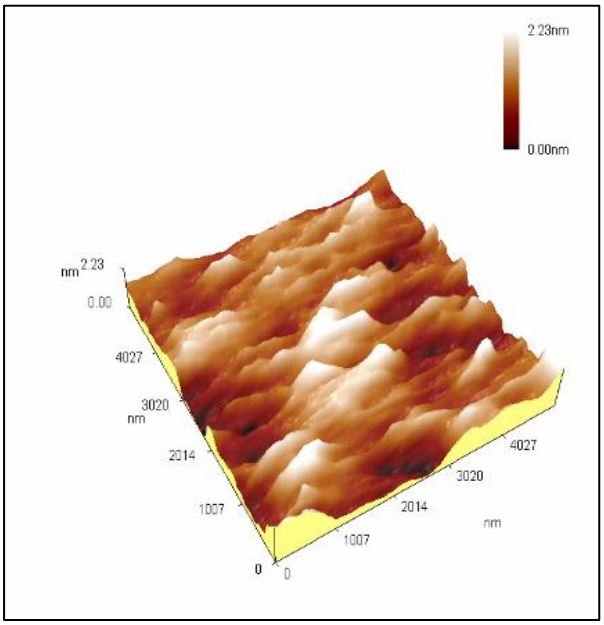

(a)

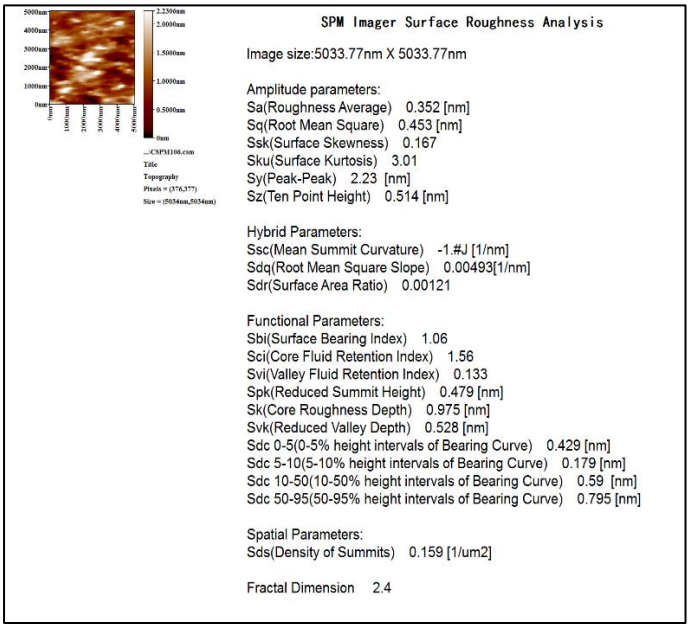

SPM Imager Surface Roughness Analysis

Image size:5033.77nm X 5033.77nm

Amplitude parameters:
Sa(Roughness Average) 0.352 [nm]
Sq(Root Mean Square) 0.453 [nm]
Ssk(Surface Skewness) 0.167
Sku(Surface Kurtosis) 3.01
Sy(Peak-Peak) 2.23 [nm]
Sz(Ten Point Height) 0.514 [nm]

Hybrid Parameters:
Ssc(Mean Summit Curvature) -1.#J [1/nm]
Sdq(Root Mean Square Slope) 0.00493[1/nm]
Sdr(Surface Area Ratio) 0.00121

Functional Parameters:
Sbi(Surface Bearing Index) 1.06
Sci(Core Fluid Retention Index) 1.56
Svi(Valley Fluid Retention Index) 0.133
Spk(Reduced Summit Height) 0.479 [nm]
Sk(Core Roughness Depth) 0.975 [nm]
Svk(Reduced Valley Depth) 0.528 [nm]
Sdc 0-5(0-5% height intervals of Bearing Curve) 0.429 [nm]
Sdc 5-10(5-10% height intervals of Bearing Curve) 0.179 [nm]
Sdc 10-50(10-50% height intervals of Bearing Curve) 0.59 [nm]
Sdc 50-95(50-95% height intervals of Bearing Curve) 0.795 [nm]

Spatial Parameters:
Sds(Density of Summits) 0.159 [1/um2]

Fractal Dimension 2.4

(b)

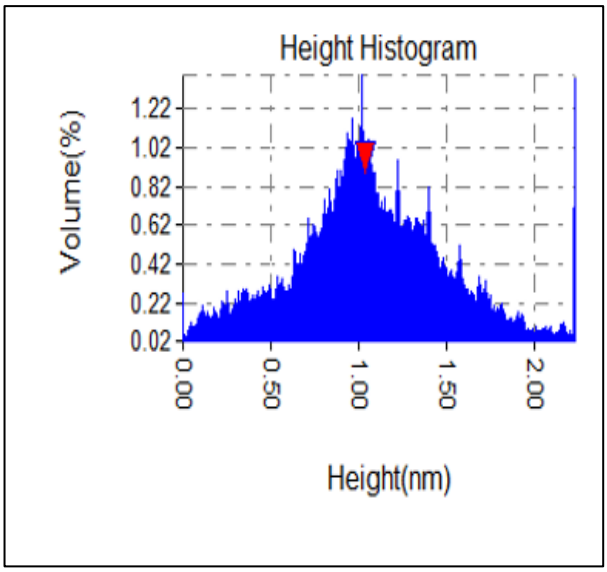

(c)

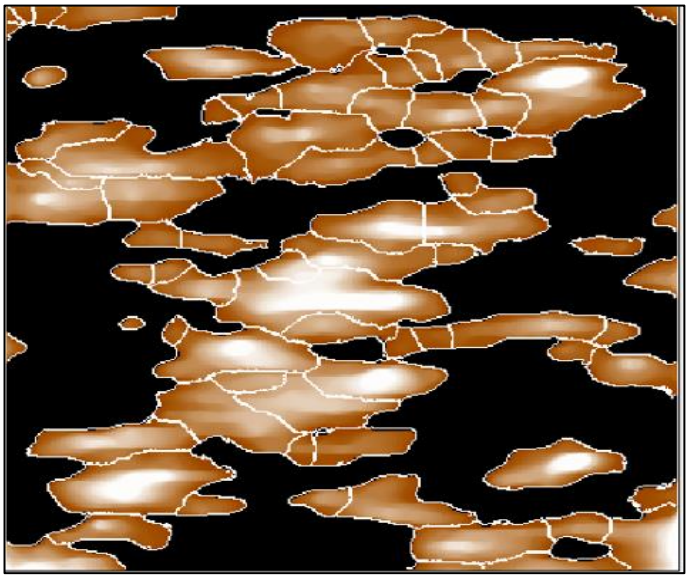

(d)

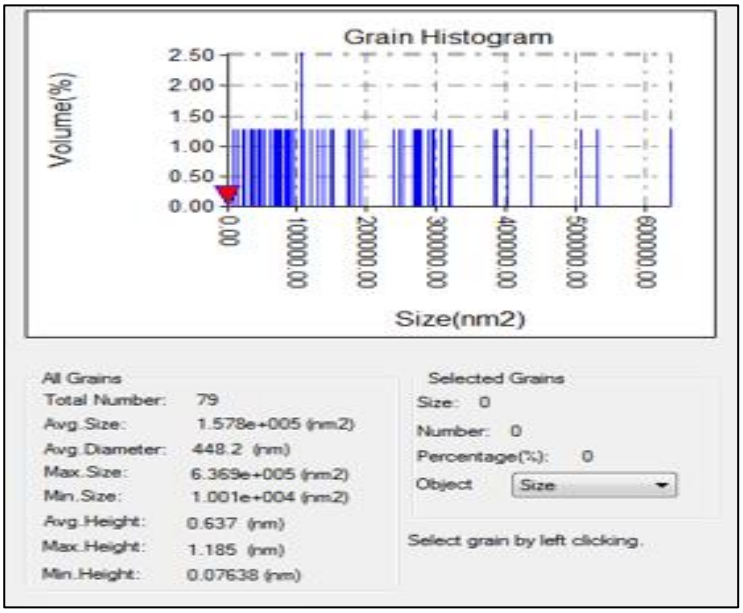

(e)

Fig.(4.5): AFM Image of Al-Ni-Cr Films with Thickness t_4 (3-layer (65 nm)) in a- 3D,b- 2D , c- Height Histogram, d- The Distribution Granular, and e- Grain Histogram.

From the figures(4.2-4.5), at the thickness increased from t_1 to t_4 it can note that the granular structure around a few nanometers with the grain size, a root mean square (RMS) ranged of (0.4-0.453)nm, roughness ranged of (0.318-0.352) nm. And a maximum peak to peak height (Sz) (ten point height) ranged of (0.682-0.514) nm, very few surface roughness and ten point height values were observed, this means that the roughness is less than nano, and this indicates that the surface is very homogeneous and this result is good to prove that the surface is a good reflector. It was observed that the values decreased at t_3, because t_3 represents two layers of

nanolayers with different weights from t_1 and t_2. The (AFM) data results were listed in table (4.1).

Table (4.1): AFM Data of Al-Ni-Cr Nano Films with Various Thicknesses.

Nano film(nm)	Roughness average Sa(nm)	Root mean square Sq (nm)	Ten point height Sz (nm)	Avg. Diameter (nm)
t_1	0.318	0.004	0.682	317.2
t_2	1.004	1.073	1.029	373.8
t_3	1.000	1.023	0.638	416.6
t_4	0.352	0.453	0.514	448.2

The figures (4.6- 4.9) refer to the curve of the relationship between the (AFM) data table and the different thicknesses of the different nanofilm layers.

Fig (4.6) represents the relationship between the rate of roughness(nm) and thicknesses(nm) of the (Al-Ni-Cr) nanofilms, where it is observed that the curve decreases with increasing thicknesses.

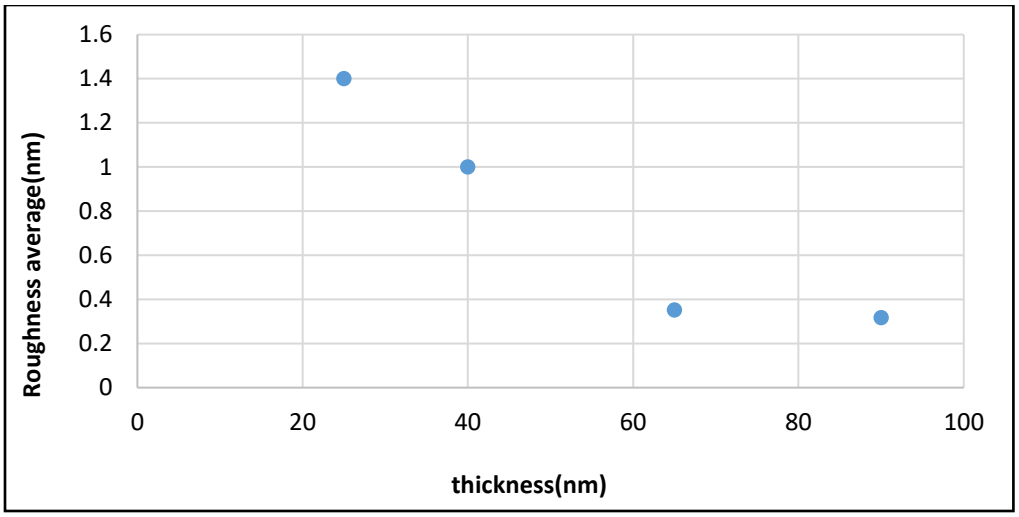

Fig.(4.6): Variation of Roughness Average Sa(nm) of Al-Ni-Cr Nano Films Measured with Various Thicknesses, where : t_1(1-layer (90 nm)), t_2(1-layer (25 nm)), t_3(2-layers (40 nm)),t_4(3-layers (65 nm)).

Fig (4.7) represents the relationship between the root mean square (sq) (nm) and thicknesses(nm) of the (Al-Ni-Cr) nanofilms, where it is observed that the curve decreases with increasing thicknesses.

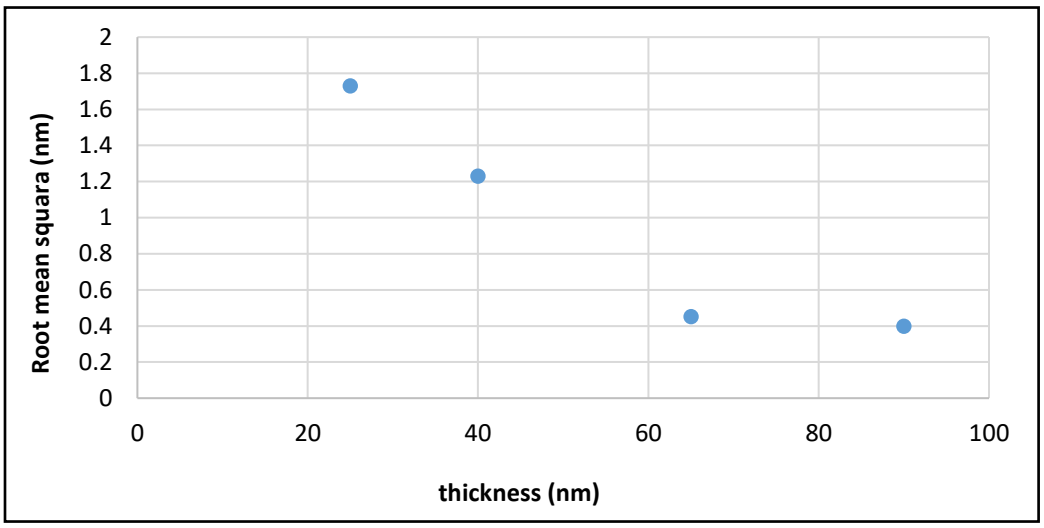

Fig.(4.7): Variation of Root Mean Square Sq (nm) of Al-Ni-Cr Nanofilms Measured with Various Thicknesses, where : t_1 (1-layer (90 nm)), t_2 (1-layer (25 nm)), t_3 (2-layers (40 nm)), t_4 (3-layers (65 nm)).

Fig (4.8) represents the relationship between the ten point height (Sz) (nm) and thicknesses (nm) of the (Al-Ni-Cr) nanofilms, where it is observed that the curve decreases with increasing thicknesses.

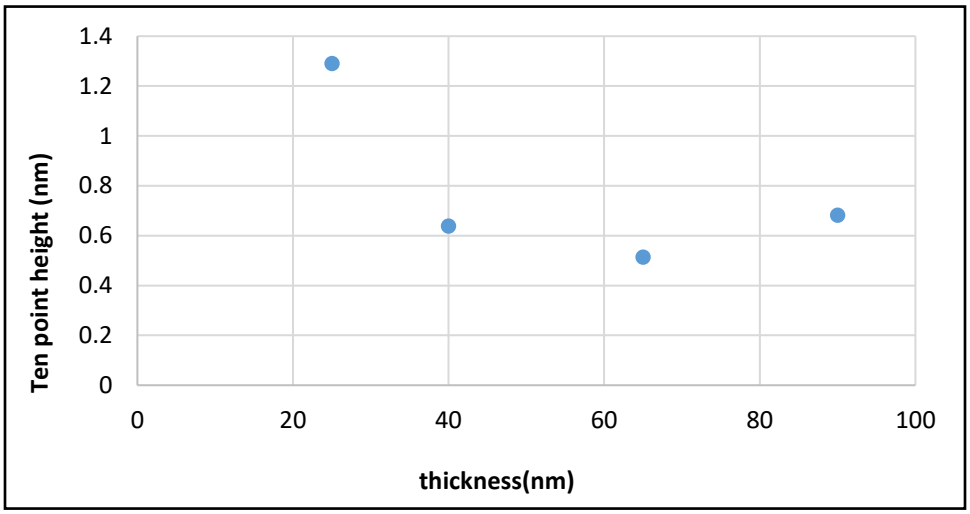

Fig.(4.8): Variation of Ten Point Height Sz (nm)of Al-Ni-Cr Nanofilms Measured with Various Thicknesses, where : t_1(1-layer (90 nm)), t_2(1-layer (25 nm)), t_3(2-layers (40 nm)),t_4(3-layers (65 nm)).

Fig (4.9) represents the relationship between the avg. diameter (nm) and thicknesses(nm) of the (Al-Ni-Cr) nanofilms, where it is observed that the curve decreases with increasing thicknesses.

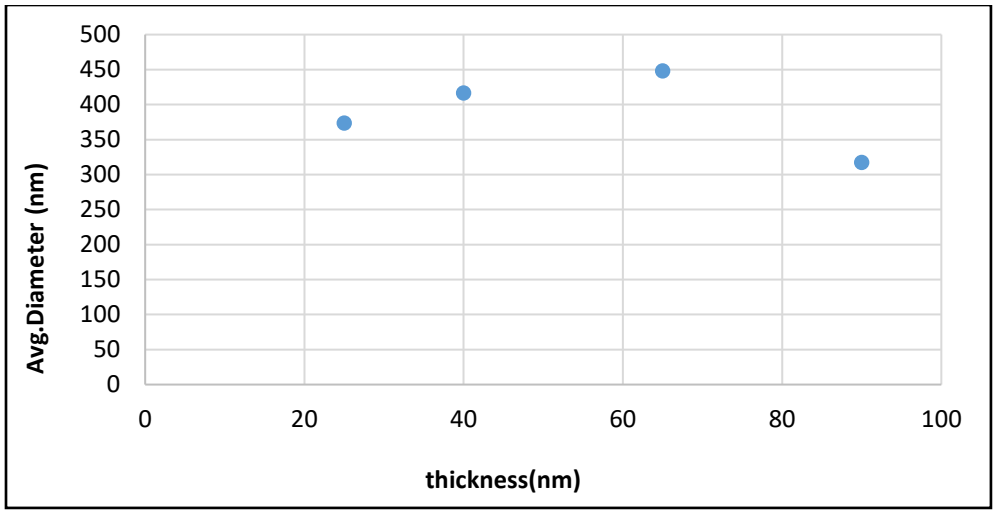

Fig.(4.9): Variation of Avg. Diameter (nm) of Al-Ni-Cr Nano Films Measured with Various Thicknesses, where : t_1(1-layer (90 nm)), t_2(1-layer (25 nm)), t_3(2-layers (40 nm)),t_4(3-layers (65 nm)).

4.2.3 Scanning Electron Microscope (SEM)

The scanning electron microscope (SEM) for scanning is an appropriate technique to study the microstructural structure of nanofilms and the image of the microstructure (SEM) showing particles on a glass substrate's surface. (SEM) images of the deposited (Al-Ni-Cr) nanofilms are shown in figure (4.10).

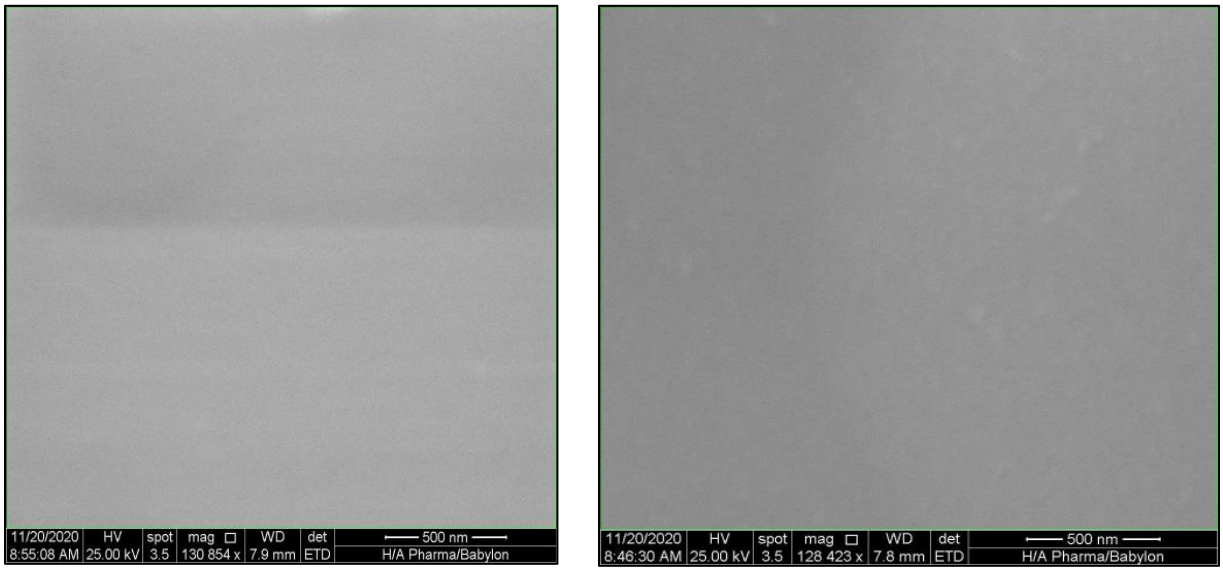

(a) **(b)**

Fig. (4.10): The SEM Images of Deposited Al-Ni-Cr Thin Films of Thickness a: t_1 (1-layer (90 nm)) and b: t_2(2-layers (40 nm)).

From Figure (4.10), the (SEM) images show that precipitated (Al-Ni-Cr) nanofilms are homogeneous, smooth, totally coated the substrate, and free from defects such as pinholes and cracks. The beans are distributed in the same size, dense, well defined. It was observed that the small spherical granules distributed over the substrate surface and it was found that the size of these grains increased with increasing thickness. Only nanocrystalline grains were observed, and the surface shapes were virtually unchanged, regardless of sedimentation time. Therefore it is difficult to obtain (SEM) images due to the small grain size. This result is similar to the published scientific research by the researchers A.Purohit,and et al [79].

4.3 Optical Properties of the (Al-Ni-Cr) Nano-Layers

In this section, the optical properties of the prepared nano films are included:

4.3.1 Reflectance

The reflectance (R) of (Al-Ni-Cr) nanofilm deposition on a glass substrate with different thicknesses were examined using two laser wavelengths; red (635 nm) and green (532 nm) by (si pin photodiode = Hamamatsu photonics USA lasers = laser diode china S1223-01). It is found that reflectance of (Al-Ni-Cr) nanofilms reached 98% for t_1 and t_4 for the 635 nm wavelength and 99% for t_1 and t_4 for 532 nm wavelength as in table (4.2). Among the main reasons for this result is the abundance of electrons on the surface, as well as, the rate of surface roughness is very low, meaning that the surface represents a smooth coating. The results refer to the possibility to use these films in reflective coatings such as laser resonators and fibers.

Table (4.2): The Reflectance of the Al-Ni-Cr Nano Films for Two Wavelengths where: t_1(1-layer (90 nm)),t_2(1-layer (25 nm)) , t_4(3-layers (65 nm)).

Thickness Thin films	Reflectivity in (635)nm	Reflectivity in (532)nm
t_1	98%	99%
t_2	83%	87%
t_4	98%	99%

4.3.2 The Transmittance

The optical transmittance as a function of wavelength in the range (200–1100) nm of (Al-Ni-Cr) nanofilms, with different thicknesses, was presented in figure (4.11).

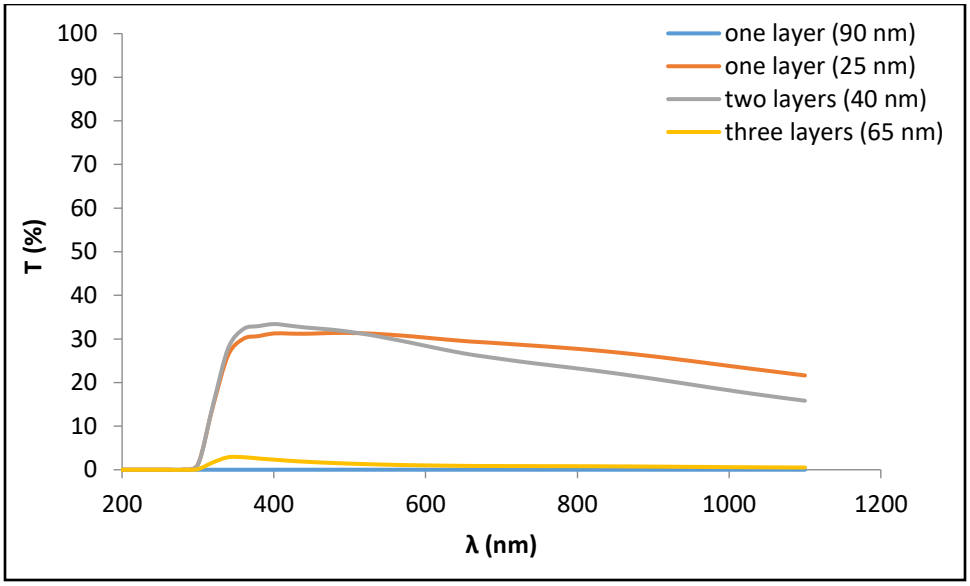

Fig.(4.11): Transmittance Spectra of Al-Ni-Cr Nano Films Measured with Various Thicknesses, where : t_1(1-layer (90 nm)), t_2(1-layer (25 nm)), t_3(2-layers (40 nm)),t_4(3-layers (65 nm)).

From figure (4.11) it observed a decrease in the transmittance with increasing wavelength. In general, figure (4.11) shows that with increasing film thickness the transmittance decreases. This behavior is due to the increase in the number of atoms of the thickness, which leads to an increase in the number of collisions between incident photon and atoms, which leads to the increase of absorbance and decreasing transmittance [80,81]. The results can compare with that of reflectance.

4.3.3 Absorbance

The optical transmission, absorption, and reflection as a function of wavelength in the range (200-1100) nm nanometers for nano-layers (different thicknesses) were measured using a visible spectrophotometer. The transmittance was measured in the

figure (4.11) and it was found that the transmittance decreases with increasing the thickness, which means that the transmittance is very low. All films show low absorbance with thickness in the visible range. This behavior can be explained as follows: At a high wavelength, the incident photon does not have enough energy to interact with the atoms. Since the absorption is less with increasing the thickness. According to the principle of the law of energy conservation (R+A+T=1), since the transmittance was measured and recorded at a very low rate of approximately 1%, and the reflectivity was recorded at 99% if the remainder from (A+R) represents the absorbance ratio (A), which is a very low percentage as in the figures (4.13-4.17).

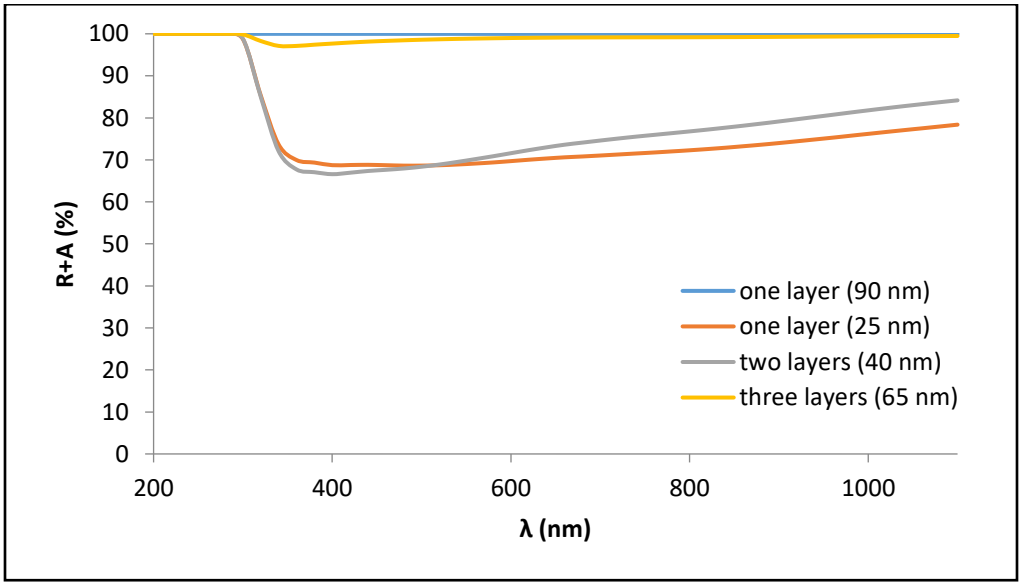

Fig.(4.12): Absorbance + Reflectance of Al-Ni-Cr Nano Films Measured with Various Thicknesses, where : t_1(1-layer (90 nm)), t_2(1-layer (25 nm)), t_3(2-layers (40 nm)),t_4(3-layers (65 nm)).

4.3.4 Dispersion Parameters and Dispersion Energies

According to the equation (2.22-24), the values of E_d, E_o, were calculated and listed in the table (4.3). From the table, the values of $E_o/2$ we get E_g. The very small values of E_g denote the conductive layer that resulted from the fabricated films, with

high reflectance because of the free electrons on the film surface. The index of refraction (n_∞) for the (Al-Ni-Cr) nano-layers was added by the interception of the perpendicular axis in Figures (4.13-4.16).

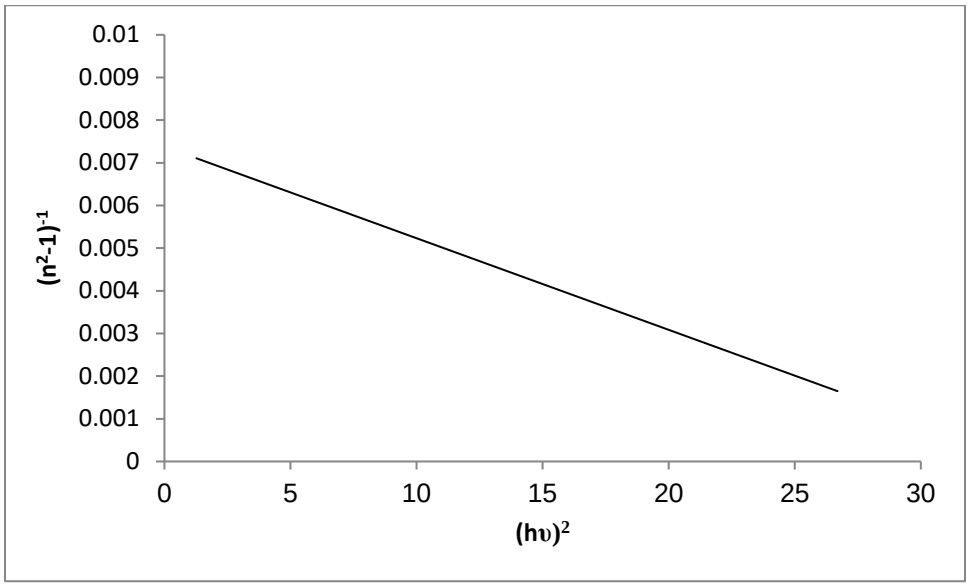

Fig. (4.13): Relationship Between $(n^2-1)^{-1}$ and $(h\upsilon)^2$ for t_1 = (90 nm).

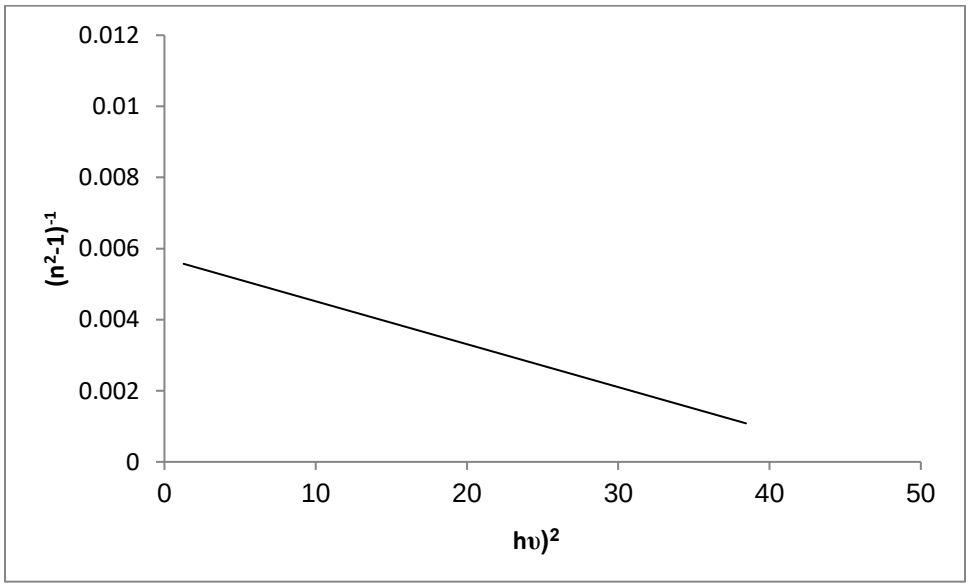

Fig. (4.14): The Relationship Between $(n^2-1)^{-1}$ and $(h\upsilon)^2$ for t_2 = (25 nm).

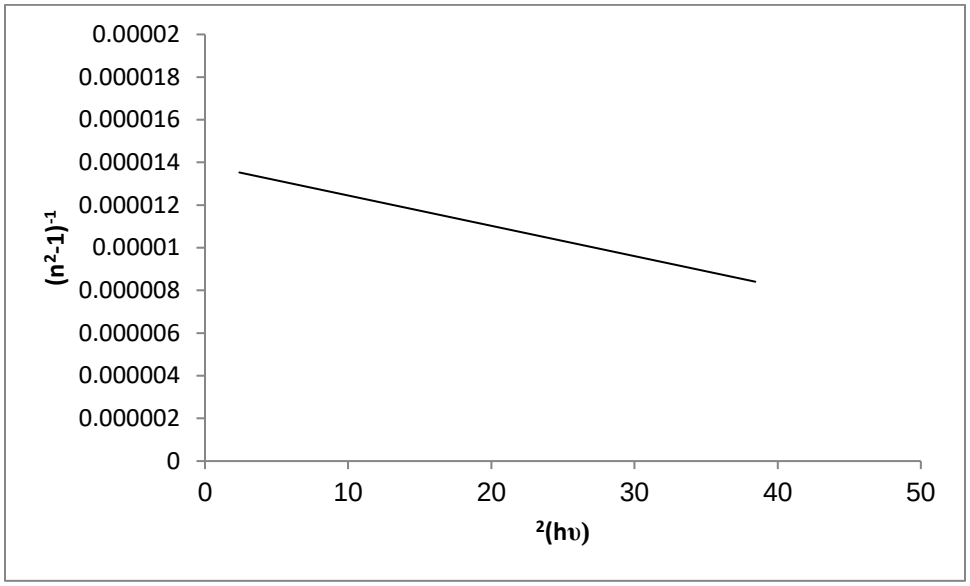

Fig. (4.15): The Relationship Between $(n^2-1)^{-1}$ and $(h\upsilon)^2$ for t_3 = (40 nm).

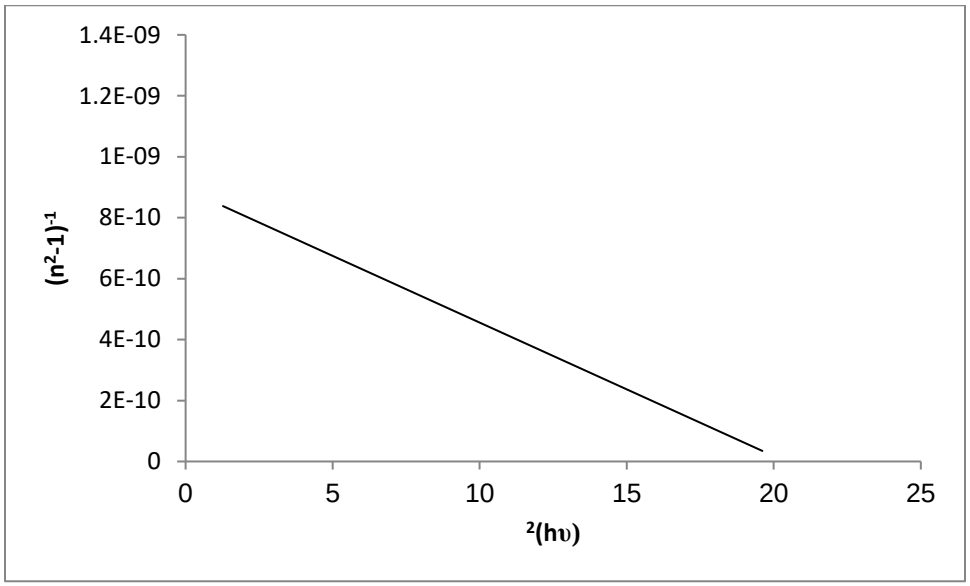

Fig. (4.16): The Relationship Between $(n^2-1)^{-1}$ and $(h\upsilon)^2$ for t_4 = (65 nm).

Table (4.3) shows the optical Parameters of Al-Ni-Cr Nano-Layers. Moments of optical perception M_{-1} and M_{-3} levels fall as the thickness of (Al-Ni-Cr) nano–layers

increases. Using the Wemple–DiDomenico process, the dispersion parameters were determined. It was noted with increasing the thickness of (Al-Ni-Cr) nano-layers, the dispersion energy (E_d) and electronic transition energy of a single oscillator (E_o) were reduced. very small values of the energy gap refer to reflective and conducted films, make them suitable in reflective and conducted devices.

Table (4.3): Optical Parameters of Al-Ni-Cr Nano-Layers.

Nano film(nm)	E_o(mev)	E_d(mev)	E_g (ev)	ε_∞	$n_{(o)}$	M_{-1}	M_{-3}
t_1	6.123	816.593	0.0030	0.1343	0.0116	4.217	0.112
t_2	6.870	1.164	0.0034	0.0011	0.0011	0.169	0.003
t_3	8.197	585.580	0.0040	0.0724	0.0085	2.259	0.033
t_4	4.609	$0.542x10^{10}$	0.0023	$1.117x10^{7}$	105.70	$0.117x10^{20}$	$0.005x10^{20}$

4.4 The Electrical Properties

The resistivity as a function of the thickness of the (Al-Ni-Cr) nanofilms is shown in Figure(4.17). The electrical resistivity of the nanofilm layers was measured by keithley. From the figure, this curve refers to the resistivity changed with the increasing the number of layers, the resistivity decreased with the increase of thickness. This shows that the (Al-Ni-Cr) nanofilms behave as a conductor as in figure (4.18). It is noticed from the study of electrical properties (electrical resistivity), (Al-Ni-Cr) nanofilms may be suitable to fabricate electrical circuits with high conductivity.

Figure (4.18) represents the electrical conductivity (the inverse of resistance) of (Al-Ni-Cr) nanofilms increased with the increase of thickness.

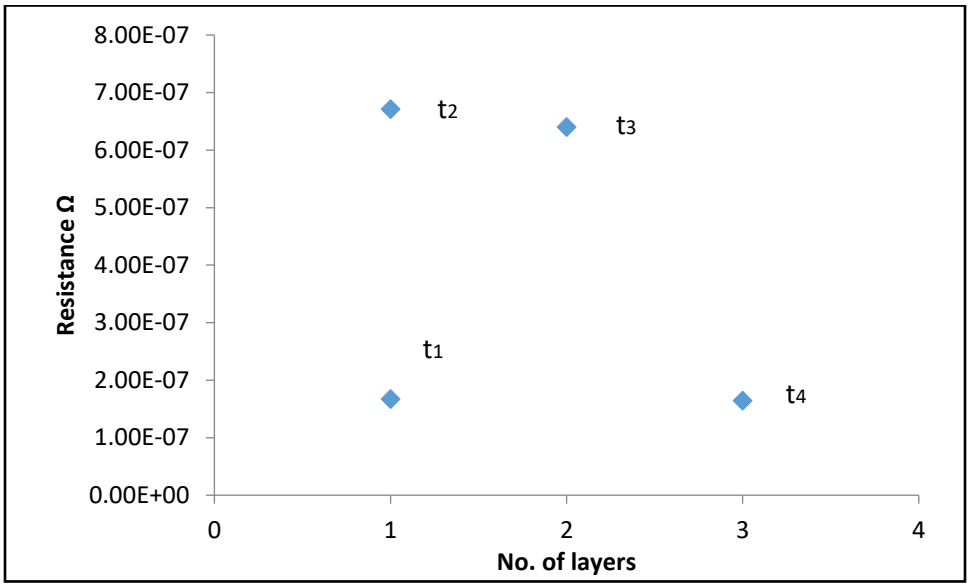

Fig.(4.17): The Electrical Resistance of Al-Ni-Cr Nano Films with Various Thicknesses, t_1(1-layer (90 nm)), t_2(1-layer (25 nm)), t_3(2-layers (40 nm)),t_4(3-layers (65 nm)).

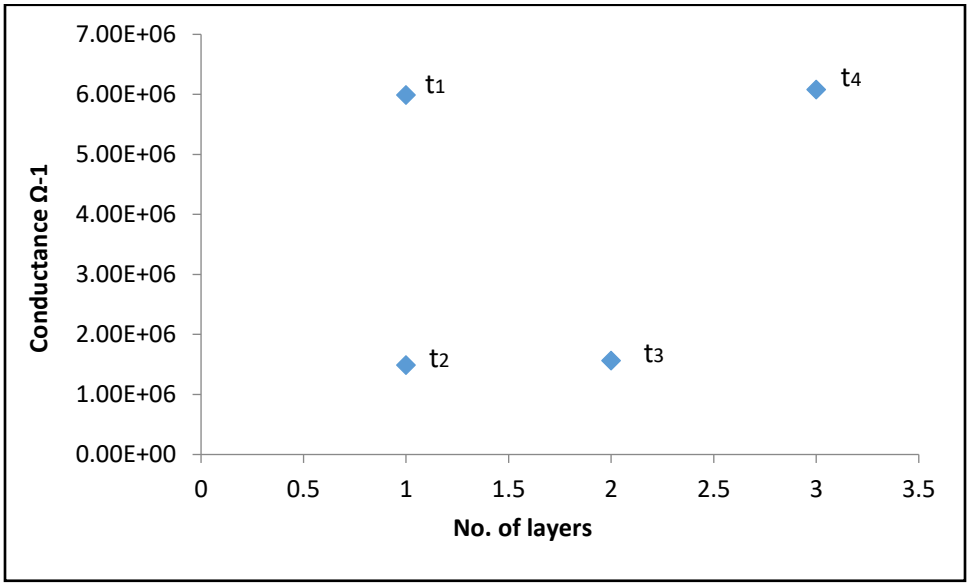

Fig.(4.18): The Electrical Conductivity of Al-Ni-Cr Nano Films with Various Thicknesses, t_1(1-layer (90 nm)), t_2(1-layer (25 nm)), t_3(2-layers (40 nm)), t_4(3-layers (65 nm)).

4.5 Conclusions

The following remarks are concluded during the present work:

1- The nanofilms formed from the deposition of the Al-Ni-Cr alloy in several layers and with different thicknesses, t_1(1-layer(90nm)), t_2(1-layer(25nm)),t_3(2-layer(40nm)),t_3(3-layer(65nm)).

2- These nanofilms is a smooth and homogeneous coating, which indicates that these films are completely reflective and conductive well.

3- The reflectance reached to 98% for t_1 and t_4 for 635 nm and 99% for the wavelength of 532 nm.

4- Using the Wemple–DiDomenico process, the dispersion parameters were determined. It was noted with increasing the thickness of (Al-Ni-Cr) nano-layers, the dispersion energy (E_d) and electronic transition energy of a single oscillator (E_o) were reduced. very small values of the energy gap refer to reflective and conducted films, make them suitable in reflective and conducted devices.

5- It is noticed from the study of electrical properties (electrical resistivity), (Al-Ni-Cr) nanofilms may be suitable to fabricate electrical circuits with high conductivity.

4.6 The Suggestions and Future Works

In this context, a further investigation can be suggested as future works:

1- Studying the effect of annealing on the structural, optical, and electrical properties of (Al-Ni-Cr) nanofilms.

2- Studying the structural, optical and electrical properties of (Al-Ni-Cr) nanofilm prepared by another method like the chemical method.

Scientific Activities

1- One research was published in an international journal (Al-SAFIR Journal).
2- One paper has been accepted for publication in scopus container .
3- The Patent is under Implementation in the Central Agency for Standardization and Quality Control.
4- Certificate of participation in the international scientific conference for advanced research in pure and applied sciences at the university of al-muthanna in partnership with the university of malaysian sciences, and a certificate of participation in the fifth international conference on chemical safety and security.
5- Participation in three electronic seminars in the department of physics, the most important of which was how to raise the level of scientific research among graduate students, as well as about the importance of publishing in international journals.
6- Participation in the scientific symposium for postgraduate students held in the faculty of science, department of physics.

References

[1] K.H.Abass, and F.SH.Hashim,. Structural and Microhardness Studies of Al-Ni-Cr Alloy Ingots. Journal of University of Babylon/ Pure and Applied Sciences, 22(4),(2014).

[2] J. L. Melville and R.G.Compton,. The Simulation of Differential Pulse Voltammetry Electroanalysis, An International Journal Devoted to Fundamental and Practical Aspects of Electroanalysis 13 (2), PP. 123-130, (2001).

[3] B . Grushko, B . Przepiorzynski , D .Pavlyuchkov,W.Kowalski and M.Surowiec. A Contribution to the Al- Ni- Cr Phase Diagram ,Journal of Alloys and Compounds 460, pp. 299-304,(2008).

[4] J. H. Fendler, and Y. Tian,. Nanoparticles and Nanostructured Films: Current Accomplishments and Future Prospects. Nanoparticles and Nanostructured Films: Preparation, Characterization and Applications , pp. 429-461,(1998).

[5] A.J.Strandjord, S.Popelar, and C.Jauernig,. Interconnecting to Aluminum-and Copper-Based Semiconductors Electroless-Nickel/Gold for Solder Bumping and Wire Bonding. Microelectronics Reliability, 42(2), pp. 265-283,(2002).

[6] K.H.Abass and M.K.Mohammed,. Fabrication of ZnO:Al/Si Solar Cell and Enhancement its Efficiency Via Al-Doping, Nano Biomedicine and Engineering, 11(2), pp. 170-177,(2019).

[7] K.H.Abass and N.H. Obaid,. 0.006wt.%Ag-Doped Sb_2O_3 Nanofilms with Various Thickness: Morphological and Optical Properties, Journal of Physics: Conference Series, 1294(2), (2019).

[8] A.N. Tuama, K. H. Abass and M. A. Agam,. Fabrication and Characterization of Cu_2O:Ag/Si Solar Cell Via Thermal Evaporation Technique, International Journal of Nanoelectronics and Materials,13(3), (2020).

[9] C.Heine and R.H.Morf,. Submicrometer Gratings for Solar Energy Applications., 34(14), pp.2476–2482. Applied Optics (1995).

[10] Y.Kanamori, E.Roy and Y.Chen,. Antireflection Sub-wavelength Gratings Fabricated By Spin-Coating Replication. Microelectron Engineering., 78-79, pp. 287–293, (2005).

[11] C.Aydin, A.Zaslavsky,G.J. Sonek and J.Goldstein,. Reduction of Reflection Losses in $ZnGeP_2$ Using Motheye Antireflection Surface Relief Structures. Applied Physice Letters 80(13), pp.2242–2244, (2002).

[12] G. Zhang, J.Zhang, J. Xie, Z. Liu and H. Shao ., Cicada Wings: A Stamp from Nature for Nanoimprint Lithography., 2(12), pp.1440–1443,(2006)

[13] G. R. Fowles and H.Richard,. Introduction to Modern Optics, Holt Richard and Winston, Inc., New York, (1968).

[14] V.Pokropivny , R.Lohmus, I.Hussainova, A.Pokropivny and S.Vlassov,. Introduction to Nanomaterials and Nanotechnology , Tartu University Press, pp. 45-100,(2007).

[15] A. Sahoo,. Synthesis and Characterization of Bio-Composite. Ph.D. Thesis, Physics Department , National Institute of Technology, (2011).

[16] H.Hahn,. Gas Phase Synthesis of Nano Crystalline Materials, Nanostructured Materials, 9(1-8),pp. 3-12, (1997).

[17] B.D.Malhotra, and M.A.Ali,. Nanomaterials for Biosensors,Fundamentals and Applications. Nanomaterials for Biosensors,1, (2018).

[18] C.Christine, and L. Goldman,. Implications of Nanotechnology for Environmental Health Research, National Academies Press, (2005).

[19] L. Kazmevski ,. Polycrystalline and Amorphous Thin Films and Devices, Academic Press ,Elsevier, (2012).

[20] O. S. Heavens,. Thin Films Physics (Science Paper Book) ,(1973).

[21] A.Merati,. A Study of Nucleation and Fatigue Behavior of an Aerospace Aluminum Alloy 2924-T3, International Journal of Fatigue, 27(1),pp. 33-44, (2005).

[22] N. A. Sevtsova and V. G. Shepelavech,.Rapidly Solidified for the Foils of Al-Ni-Cr Alloys System, Minsk, pp. 8-13, (2006).

[23] D. N. Compton, L. A. Coornish, and M. J. Witcomb,. The Effect of Microstructure on Hardness Measurements in the Aluminum-Rich Corner of the Al-Ni-Cr System, Journal of Alloys and Compounds, 317,pp. 372-378, (2001).

[24] V. Raghavan,. Al-Cr-Ni (Aluminum-Chromium-Nickel), Journal of Phase Equilibria and Diffusion,Springer, 30,pp. 61-63, (2009).

[25] R. Rossetti, L. Ellison, S. M. Gibson, and L. E. Bruse,.Size Effects in the Excited Electronic States of Small Colloidal CdS Crystallites Journal of Physical Chemistry,80, p. 4464, (1984).

[26] W.Kowalski, B.Grushko, D.Pavlyuchkov, and M. Surowiec,. A contribution to the Al–Pd–Cr Phase Diagram. Journal of Alloys and Compounds, 496 (1-2), pp. 129-134,(2010).

[27] M.Gojic, L.Vrsalovic, S.Kozuh, A.Kneissl, I.Anzel, S.Gudic, and M.Kliskic,. Electrochemical and Microstructural Study of Cu–Al–Ni Shape Memory Alloy, Journal of Alloys and Compounds, 509(41), pp. 9782-9790,(2011).

[28] K.H.Abass and F.SH.Hashim,. Novel Preparation of Antireflection Nanofilms from Al-Ni-Cr Alloy , British Journal of Science,7(1) ,(2012).

[29] Z.Sun, C.H.Liebscher, S.Huang, Z.Teng, G.Song, G.Wang, and P.K.Liaw,. New Design Aspects of Creep-Resistant NiAl-strengthened Ferritic Alloys. Scripta Materialia, 68(6), pp. 384-388,(2013).

[30] C.M.Chang, C.H.Wang, J.H.Hsu, and J.C.Huang,. Al–Ni–Y–X (X= Cu, Ta, Zr) Metallic Glass Composite Thin Films for Broad-Band Uniform Reflectivity. Thin Solid Films, 571, pp. 194-197,(2014).

[31] K. H. Abass, and Sh. L. Hamdan,. Effect of Thickness on the Optical Properties of Al-Ni-Cr Thin Films Prepared by Thermal Evaporation Technique. International Journal 3.12 : pp. 369-374,(2015).

[32] V. G. Shmorgun, A. Bogdanov, and A.O. Taube,. Effect of the High-Heating on the Chemical and Phase Composition of the Al-Ni-Cr Layered Coatings. Materials Science Forum870,pp. 169-174, (2016).

[33] P.Pandey, S.Kashyap, C.S.Tiwary, and K.Chattopadhyay,. Development of High-Strength High-Temperature Cast Al-Ni-Cr Alloys Through Evolution of a Novel Composite Eutectic Structure. Metallurgical and Materials Transactions A, 48(12), pp. 5940-5950,(2017).

[34] M.Kawamura, T.Kiba, Y.Abe, K.H.Kim, and H.Murotani,. Metal Nanolayer Deposited Highly Stable Ag Thin Films and their Optical Properties. In Journal of Physics: Conference Series 987, IOP Publishing,(2018).

[35] K.M.Oluwasegun, O.O.Ajide, T.Tanaka, L.Zhang, and O.A.Ojo,. Hot Corrosion Performance of Single-Crystal CMSX-4 and CMSX-486 Superalloys in the Mixture of Na_2SO_4-NaCl Melts. Journal of Materials Engineering and Performance, Springer 28, pp.5509-5520,(2019).

[36] T.Stefanov,H.V.R.Maraka, P.Meagher, J.Rice, W.Sillekens, and D.J.Browne,. Thin Film Metallic Glass Broad-Spectrum Mirror Coatings for Space Telescope Applications, Journal of Non-Crystalline Solids: ,7,(2020).

[37] D.Aryanto, H.Hariyati, P.K.Karo, A.S.Wismogroho, W.BWidayatno, A.Basyir, and A.Noviyanto,. Microstructure and Oxidation Behavior of an Al–Ni–Cr–Cu–MoO_3–SiO_2 Composite Coating on Low-Carbon Steel. Materials Chemistry and Physics, 261, p.124250,(2021).

[38] M. Fox,. Quantum optics, an introduction, OUP Oxford,15, (2006).

[39] A.Guinier, X-ray Diffraction in Crystals, Imperfect Crystals, and Amorphous Bodies, Freeman, San Francisco,(1963).

[40] J. Als-Nielsen and D. McMorrow, Elements of Modern X-ray Physics, John Wiley and Sons, Ltd., Chichester,(2001).

[41] C. S. Barrett and T.B. Massalski,. Structure of Metals, Mc Graw-Hill, New York, (1966).

[42] A.Singh, D. Khanna, P. K. Khanna, B. C. Joshi , and M. Kumar,. Effect of Post Annealing Temperature on Structural and Optical Properties of ZnCdO Thin Films Deposited by Sol–Gel Method, Applied Surface Science, 258(5), pp. 1881-1887, (2011).

[43] A. Yousif, Structural, Morphological, photo-Properties of Hetrojunction ZnO Nanostructure Films Deposited on n-Si(100)by PLD, IJAIEM,3, pp. 44-55, (2014).

[44] H. Moharram, S. A. Mansour, M. A. Hussein, and M. Rashad,. Direct Precipitation and Characterization of ZnO Nanoparticles, Journal of Nanomaterials,(2014).

[45] A.Singh and P. Kumar,. Structural, morphological and optical properties of sol- gel processed CdZnO nanostructured films: effect of precursor solvents, International Nano Letters, 3(1), pp. 1-6, (2013).

[46] A. Efros and B. I. Shklovskii,. Critical Behaviour of Conductivity and Dielectric Constant Near the Metal-Non-Metal Transition Threshold, Physical Status Solid (b), 76(2), pp. 475-485, (1976).

[47] I.vashchenko and I. Kerner ,. Physical Approaches to Improvement of Semiconductor Gas Sensor Based on SnO_2 Thin Films, Moldavian Journal. of the Physical Sciences, No.1, pp. 95-102, (2003).

[48] E. Meyer, Atomic Force Microscopy, Progress in Surface Science,41(1), pp. 3-49, (1992).

[49] A.Said, L. Sajti, S. Giorgio, and W. Marine,. Synthesis of Nanohybrid Materials by Femtosecond Laser Ablation in Liquid Medium, IOP Publishing Journal of Physics, Conference Series, 59(1), p.055, (2007).

[50] C. E. Lyman, D. E. Newbury, J. I. Goldstein, D. B. Williams, A. D. Romig, J. T.Armstrong, P. Echlin, C. E. Fiori, D. C. Joy, E. Lifshin and K. Peters,. Coating Methods ,. Scanning Electron Microscopy, X-Ray Microanalysis and Analytical Electron Microscopy: A Laboratory Workbook. Plenum Press. New York,pp. 180-186, (1990).

[51] H. S. Nalwa,. Hand Book of Thin Films ,Five Volume Set, Elsevier , (2001).

[52] B.G. Strectman. and S. Banerjee,. Solid State Electronic Devices, 5th. Ed., Engle Wood Cliffs, Prentice Hall, (2000).

[53] O. Stenzel,.The Physics of Thin Film Optical Spectra Surface Sciences, Springer,Berlin, (2005).

[54] K. Gabur, Preparation and Study the Electrical and Optical Properties of (PS-Ni) Composites, M.Sc. Thesis, Babylon University, College of Science, (2010).

[55] R. D. Shannon and J. A. Pask,. Kinetics of the Anatase-Rutile Transformation, Journal of the American Ceramic Society, 48(8) ,pp. 391-398, (1965).

[56] T. Nishimori, K. Nakano,H.Sakamoto,Y.Takakuwa and S.Kono,.n–type High–Conductive Epitaxial Diamond Film Prepared By Gas Source Molecular Beam Epitaxy with Methane and Tri-n- Butylphosphine, Applied Physics Letters, 71(7),pp. 945–947, (1997).

[57] G. B .Palmer, K. R. Poeppelmeier, and T. O. Mason,.Conductivity and Transparency of ZnO/SnO_2–Cosubstituted In_2O_3, Chemistry of Materials,9(12), pp. 3121–3126, (1997).

[58] Sh. L. Hamdan,. Investigation of Some Physical Properties of Thin Films Prepared From Al-Ni-Cr Alloy, M.Sc.Thesis, University of Babylon, (2016).

[59] M. A. Omar,. Elementary Solid State Physics, Principles and Applications,Pearson Education India, (1975).

[60] J. L. Vossen , W. Kern and W.Kern ,. Thin Film Processes II. Gulf Professional Publishing , (1991).

[61] J. M. Lafferty,.Vacuum: from Art to Exact Science. Physics Today,34(11), pp. 211-31, (1981).

[62] R. W. Bery, P. M. Hall and M. T. Harris,. Thin Film Technology. D.Van Nostrand Reinhold Company,1968,706 P, (1968).

[63] D.M. Mattox and V.H.Mattox ,. Vacuum Coating Technology, Springer , (2003).

[64] K.N.Jha and N.D.Taneja ,.Vacuum Deposition Plant for Thin Film Circuit,IETE Journal of Research 12 (9),pp. 478-483 ,(1966).

[65] S. M. Sze and S.M.Sze ,. Selected Solutions for Semiconductor Devices Physics and Technology, Wiley , (1985).

[66] D.A.Neaman,. Semiconductor Physics and Devices, Basic Principles, Richard D. Irwin Inc.,Boston, (1992).

[67] B.G. Streetman and S.K.Banerjee ,. Solid state Electronic Devices ,$6^{th.}$ Ed. Prentice –Hall India New Delhi, (2006).

[68] A .G. Milne and F. L. Feucht,.Hetrojunction and Metal Semiconductor Junction, Academic Press, New York and London, (1972).

[69] J. Wilson and J. F. B. Hawkes,.Optoelectronics An Introduction, 2nd. Ed.,(1989).

[70] E.S.Field, J.C.Bellum, and D.E. Kletecka,. Repair of a Mirror Coating on a Large Optic for High Laser Damage Applications Using Ion Milling and Over-Coating Methods. Optical Engineering, 56(1), p. 011002,(2016).

[71] R.Paschotta,. Encyclopedia of Laser Physics and Technology, Wiley-VCH, (2016).

[72] I. Stevenson C. Boone ,. Laser Mirrors: High Reflectance is Measured Best With Cavity Ring-Down Spectroscopy, 55(4), pp. 37-40, (2019).

[73] F.A. Jenkins, H.E. White,. Fundamentals of Optics, Indian Journal of Physics 25, pp. 265-266, (1957).

[74] S.H.Wemple and M.DiDomenico Jr,. Behavior of the Electronic Dielectric Constant in Covalent and Ionic Materials, Physical Review Journals B 3(4), p.1338(1971).

[75] S.H.Wemple,. Refractive-Index Behavior of Amorphous Semiconductors and Glasses, Physical Review Journals B 7(8), p. 3767(1973).

[76] A.S.Hassanien, and A.A.Akl,. Influence of Composition on Optical and Dispersion Parameters of Thermally Evaporated Non-Crystalline $Cd_{50}S_{50-x}Se_x$ Thin Films. Journal of Alloys and Compounds, 648, pp.280-290(2015).

[77] K.H.Abass, D.M.A.Latif,. The Urbach Energy and Dispersion Parameters Dependence of Substrate Temperature of CdO Thin Films Prepared By Chemical Spray Pyrolysis, International Journal of ChemTech Research, 9(9), pp. 332-338, (2016).

[78] K. H. Abass,.Preparation and Study Structural, Optical, and Electrical Properties of Al-Ni-Cr Thin Film, Al–Mustansiriyah University, Ph.D. Thesis, (2012).

[79] A.Purohit, S.Chander, S.P.Nehra, C. Lal, and M.S. Dhaka,. Effect of Thickness on Structural, Optical, Electrical and Morphological Properties of Nanocrystalline CdSe Thin Films for Optoelectronic Applications. Optical Materials, pp. 345-353,(2015).

[80] Y. Y. Peter and M. Cardona,. Fundamentals of Semiconductors, Physics and Materials Properties Springer-Verlag Berlin Heidelberg, New York, (2005).

[81] P. Kay and Johnson,. The Effect of Trapping Defects on CIGS Solar-Cell Performance, Doctoral Diss., Colorado State University, USA, (2003).

ICARPAS 2021.
AIP Conf. Proc .

Ref. No. ICARPAS-PHYS-73
Dated: 20/3/2021

Publication Acceptance Letter

Manuscript ID: ICARPAS-PHYS-73

Authors: Huda R. Abdulridha Mohammed, Abdulazeez O. Mousa Al-Ogaili, Khalid Haneen Abass

Corresponding Author: Huda R. Abdulridha Mohammed

Affiliation: Department of Physics, College of Science, University of Babylon, Iraq.

Dear (authors)

We are pleased to inform you that, after peer- review process, your manuscript entitled:

"Synthesis and Structural Characterization of Nano-layers Prepared from Al-Ni-Cr Alloy for Reflectance Coatings"

has been accepted for presentation and publishing in the "**1st International Conference on Advanced Research in Pure and Applied Science**", which will be held at College of Science / Al- Muthanna University, Iraq during 24-25 March, 2021. Your paper will be published online by **AIP Conference Proceedings (ISSN: 0094-243X).**

Your interest in ICARPAS 2021 is very much appreciated. We look forward to meet you at this event.

With Best Regards,

Prof. Dr. Laith Abdul Hassan M. Jawad
Chairman of ICARPAS 2021

Materials Today: Proceedings

Available online 24 July 2021

In Press, Corrected Proof

Structural and dispersion parameters of nano-layers prepared from Al-Ni-Cr alloy

Huda R. Abdulridha Mohammed [a], Abdulazeez O. Mousa Al-Ogaili [a], Khalid Haneen Abass [b]

[a] Department of Physics, College of Science, University of Babylon, Iraq

[b] Department of Physics, College of Education for Pure Sciences, University of Babylon, Iraq

Available online 24 July 2021.

الخلاصه

في هذه الدراسة ، طبقات نانويه من سبيكة (Al-Ni-Cr) بسمك مختلف (طبقة واحدة (٩٠ نانومتر) طبقة واحدة (٢٥ نانومتر) ، طبقتان (٤٠ نانومتر) ، ٣ طبقات (٦٥ نانومتر)) ، باستخدام تقنية التبخير الحراري على ركائز زجاجية تحت ضغط ١٠-٧ ملي بار. وقد لوحظ من خلال النتائج أن بنية هذه الأفلام كانت غير متبلورة ولا يوجد اتجاه للأفلام. لا تظهر أي قمم تشير إلى بنية بلورية دقيقة جدًا من اختبار (XRD)وسطح الأغشية الرقيقة لسبائك (Al-Ni-Cr) متجانسة وناعمة ومغلفة تمامًا وخالية من العيوب مثل ثقوب الدبوس والشقوق. يتم توزيع الحبوب بنفس الحجم ، كثيفة ، ومحددة جيدًا. لوحظ أن الحبيبات الكروية الصغيرة موزعة على سطح الركيزة ووجد أن حجم هذه الحبوب يزداد مع زيادة السمك. لوحظنا حبيبات متناهية الصغر فقط ، ولم تتغير أشكال السطح تقريبًا ، بغض النظر عن وقت الترسيب ، لذلك من الصعب الحصول على صور SEM بسبب حجم الحبوب الصغير من اختبارات (SEM و AFM) .تمت دراسة الخواص الضوئية للأغشية الرقيقة لسبائك (Al-Ni-Cr) بشكل أساسي عن طريق تسجيل أطياف النفاذية باستخدام مقياس طيف ضوئي مرئي للأشعة فوق البنفسجية في حدود (٢٠٠-١١٠٠) نانومتر. من هذه الأطياف ، لاحظت انخفاضًا في النفاذية مع زيادة الطول الموجي. بشكل عام ، مع زيادة سمك الفيلم تقل النفاذية. يرجع هذا السلوك إلى زيادة عدد ذرات السمك ، مما يؤدي إلى زيادة عدد الاصطدامات بين الفوتون الساقط والذرات ، مما يؤدي إلى زيادة الامتصاصية وتقليل النفاذية. يمكن مقارنة النتائج بنتائج الانعكاس. تقل النفاذية مع زيادة السمك ، بينما تدرس انعكاسية الأغشية النانوية باستخدام ٦٣٥ نانومتر وطول موجي ليزر ٥٣٢ نانومتر. وصل الانعكاس إلى ٩٨٪ للسمك الاول t_1 و للسمك الرابع t_4 للطول الموجي ٦٣٥ نانومتر و ٩٩٪ للطول الموجي ٥٣٢ نانومتر. تشير النتائج إلى إمكانية استخدام هذه الأغشية في الطلاءات العاكسة مثل مرنان الليزر والألياف. تم حساب معاملات التشتت باستخدام عمليات Wemple – DiDomenico يتم تقليل طاقة المذبذب الفردي للانتقال الإلكتروني (E_o) وطاقة التشتت (E_d) مع زيادة سمك الطبقة. تحتوي الأفلام العاكسة والمنفذة على قيم فجوة طاقة صغيرة جدًا. تم فحص الخواص الكهربائية لأغشية-Al-Ni) (Crالرقيقة بشكل أساسي من خلال قياسات الموصلية. هذا يدل على أن أغشية Al-Ni-Cr الرقيقة تتصرف كموصل. لوحظ من دراسة الخواص الكهربائية (المقاومة الكهربائية) أن الأغشية النانوية Al-Ni-Cr قد تكون مناسبة لتصنيع الدوائر الكهربائية ذات الموصلية العالية.

وزارة التعليم العالي و البحث العلمي
جامعة بابل
كلية العلوم
قسم الفيزياء

طبقات نانوية عالية الانعكاس محضرة من سبيكة (المنيوم- نيكل- كروم) لمرنان الليزر بوساطة تقنية التبخير الحراري

رسالة

مقدمة الى مجلس قسم الفيزياء - كلية العلوم - جامعة بابل وهي جزء من متطلبات نيل درجة الماجستير في العلوم / الفيزياء

من قبل

هدى رعد عبد الرضا محمد

بكالوريوس علوم فيزياء / ٢٠١٧

بإشراف

الاستاذ الدكتور
عبد العزيز عبيد موسى العگيلي

الاستاذ الدكتور
خالد حنين عباس حسن

١٤٤٣هـ

٢٠٢١م